Published OnlineFirst October 13, 2014; DOI: 10.1158/1535-7163.MCT-14-0462

Organisation-European Society for Medical Oncology (ECCO-ESMO) 2013, no benefit was observed in *KRAS*-mutant patients (7, 8). In addition, an original study by Munshi and colleagues (3) showed that tivantinib inhibited the cell growth of *KRAS*-mutated A549 cells that had been reported to be insensitive to another c-MET inhibitor, PHA-665752 (9, 10). These results suggest that tivantinib shows cytotoxic activity in addition to c-MET inhibition. Furthermore, we and Basilico and colleagues independently reported that tivantinib showed cytotoxic activity in various cancer cells by disrupting microtubule function independent of cellular c-MET status (11–13). Related to the report (13), there is published letter explaining that the activity of tivantinib in clinical trials is related to the MET inhibition; however, there is the counterargument (14, 15). In addition, recently Remsing Rix and colleagues (16) reported that tivantinib bound and inhibited glycogen synthase kinase 3 (GSK3) alpha and beta to a greater degree than did c-MET. Molecular target of tivantinib is still uncertain.

Because microtubules have a crucial role in cancer cell division and motility, microtubules have been recognized as highly attractive targets for cancer chemotherapy. Tubulin binding agents, such as vincristine and paclitaxel, have been commonly used as chemotherapeutic drugs in various cancers. However, as with all chemotherapeutic agents, the appearance of drug-resistant cells is a major obstacle. It has been reported that microtubule inhibitor–treated cells acquired resistance through various mechanisms, including overexpression of βIII-tubulin, alteration of the β-tubulin gene, and overexpression of ABC transporters, such as P-glycoprotein (17–20). Thus, to overcome chemoresistance to tubulin binding agents, a new class of microtubule-targeting agents is currently being evaluated in clinical trials, and several drugs have recently been approved and used clinically. For example, microtubule-stabilizing agent ixabepilone, which is an analogue of epothilone B, was approved by the FDA in 2007 for treatment of patients with metastatic or advanced breast cancer whose tumors are resistant or refractory to anthracyclines, taxanes, and capecitabine. Ixabepilone showed low susceptibility against taxane-resistant cells caused by overexpression of P-glycoprotein *in vitro* and *in vivo* (21). Eribulin, a synthetic analogue of halichondrin B, has been approved by the FDA for treatment of patients with metastatic breast cancer who have previously received at least two chemotherapeutic regimens to treat metastatic disease. It has been reported that the underlying mechanism of eribulin activity is unique and that the drug suppressed the growth rates of microtubules, but unlike vinblastine, eribulin did not affect shortening rates of microtubules (22).

In the present study, we aimed to elucidate the mechanism underlying the cytotoxic activity of tivantinib in which cellular microtubules are disrupted. To determine if tivantinib shows cytotoxic activity by inhibition of tubulin polymerization, we quantified assembled microtubules in cells and a xenograft model. To determine if tivantinib directly binds to tubulin, we performed a tubulin binding competition assay using tivantinib and other ^{3}H-labeled microtubule inhibitors. We found that tivantinib directly bound to tubulin and competitively inhibited binding of colchicine to tubulin. We also used computational modeling to predict a structural model of the tubulin–tivantinib complex in the colchicine binding pocket of α- and β-tubulin complexes. On the other hand, tivantinib showed cytotoxic activity against ATP-binding cassette sub-family B member 1 (MDR1)-overexpressing cells that acquired resistance to vincristine, vinblastine, and colchicine. Tivantinib equally inhibited growth and induced apoptosis in ATP-binding cassette sub-family C member 1 (MRP1)- or ATP-binding cassette sub-family G member 2 (BCRP)-overexpressed cells. These results suggest that tivantinib, differently from other tubulin inhibitors, might be effective against multidrug-resistant cells that overexpress ABC transporters.

Materials and Methods

Cell lines and reagents

EBC-1, SK-MEL-28, DLD-1, K562, K562/VCR, CEM, and CEM/VBL were cultured in RPMI-1640 medium with 10% FBS. 293T, KB3-1, KB3-1 MDR1, KB3-1 MRP1, and KB3-1 BCRP were cultured in RPMI medium with 10% FBS. All cells were maintained at 37°C in a humidified atmosphere at 5% CO_2. EBC-1 and CEM cells were obtained from the Japanese Cancer Research Resources Bank, SK-MEL-28 was obtained from the ATCC, and 293FT was purchased from Invitrogen. K562/VCR and CEM/VBL were established in our institute (23, 24). KB3-1 cells were provided by Dr. I. Pastan (National Cancer Institute), and MDR1-, MRP1-, or BCRP-expressing subclones were provided by Dr. Y. Sugimoto (Keio University, Japan). K562 and DLD-1 cells were provided by Drs. E. Ezaki and T. Tsuruo in our institute, respectively. SK-MEL-28, DLD-1, K562, K562/VCR, 293T, KB3-1, KB3-1 MDR1, KB3-1 MRP1, and KB3-1 BCRP cells were authenticated by short tandem repeat analysis. CEM and CEM/VBL cells have not been tested by the authors. Tivantinib (ARQ 197) and crizotinib were purchased from ChemieTek. Vincristine, vinblastine, colchicine, and paclitaxel were purchased from Sigma. Streptavidin-coated yttrium scintillation proximity assay (SPA) beads, [^{3}H]colchicine, and [^{3}H]vincristine were purchased from PerkinElmer. [^{3}H]vinblastine was purchased from American Radiolabeled Chemicals. The CSII-EF-MCS vectors encoding mCherry-hCdt1 and mVenus-hGem were kindly provided by Dr. Atsushi Miyawaki (RIKEN).

Time-lapse imaging

Lentiviral plasmid for fluorescent ubiquitination-based cell cycle indicator (Fucci) expression [mCherry-hCdt1 (30/120) or mVenus-hGem (1/110)] was transfected by using a packaging plasmid into 293FT cells (25). Both viral solutions were prepared and infected into EBC-1 or SK-MEL 28 cells. Fucci-expressed clones were obtained by

Published OnlineFirst October 13, 2014; DOI: 10.1158/1535-7163.MCT-14-0462

limiting dilution. For time-lapse fluorescence microscopy, Fucci-expressing cells were plated onto a 35-mm glass-bottom dish. After 24 hours, the medium was replaced with drug-containing medium, and dishes were placed in 37°C humidified chamber of an FV10i confocal laser microscope (Olympus).

Immunoblot analysis

Cell lysates were prepared as described previously (11, 26). Equal amounts of lysates were electrophoresed and immunoblotted with the antibodies against phospho-c-MET (Tyr1234/1235) (3D7), c-MET (25H2), phospho-p42/44 ERK/MAPK (Thr202/Tyr204), p42/44 ERK/MAPK, phospho-AKT (Ser473) (D9E), panAKT (C67E7), β-actin (13E5), cleaved PARP (Asp214; Cell Signaling Technology), MDR1 (C219; MILLIPORE), MRP1 (MONOSAN), BCRP (C219; Santa Cruz Biotechnology), and α-tubulin (DM1A; Sigma). An ECL Prime Western Blotting Detection Reagent (GE Healthcare) or SuperSignal West Femto Maximum Sensitivity Substrate (Thermo Scientific) was used to detect immunoreactive signal.

Measurement of in-cell microtubule assembly

Separation of polymerized tubulin from tubulin dimmers and analysis of the effect of tivantinib on tubulin polymerization in cells were performed as described previously with some modification (27). In brief, EBC-1 or DLD-1 cells were treated with the indicated concentrations of agents. After treatment, the cells were washed with PBS, and subsequently lysis buffer containing 20 mmol/L Tris-HCl, pH 8.6, 1 mmol/L $MgCl_2$, 2 mmol/L EGTA, 1 mmol/L PMSF, 20 μg/mL aprotinin, and 0.5% Nonidet P-40 (tubulin detection buffer) was added to the treated agents. Supernatants were collected after centrifugation at 15,000 rpm for 15 minutes at 4°C. The pellets were dissolved in a Laemmli Sample Buffer. Equal amounts of supernatants and dissolved pellets were electrophoresed and immunoblotted with the indicated antibodies.

Xenograft studies

Six-week-old female athymic nude mice (Charles River Laboratory) were inoculated s.c. at 1×10^6 EBC cells per mouse. Five days after inoculation, tivantinib was administered at 200 mg/kg twice per day for 5 consecutive days, followed by a 2-day dosing holiday. Mouse body weight and tumor volume ($0.5 \times \text{length} \times \text{width}^2$) were measured twice per week. Tivantinib was formulated in polyethylene glycol 400/20% Vitamin E tocopheryl polyethylene glycol succinate (60:40) at 30 mg/mL as previously described (3). The nonparametric Mann–Whitney *U* test was used to perform statistical analysis. Nineteen days after drug treatment, the tumors were resected from the nude mice and homogenized with tubulin detection buffer (above). Cell lysates were filtered through a 0.80-μm filter, centrifuged, and subsequently immunoblotted according to the same protocol described above. All animal procedures were performed according to protocols approved by the Japanese Foundation for Cancer Research Animal Care and Use Committee.

[^{3}H]colchicine–tubulin binding assay

The tubulin binding assay was performed as reported previously with slight modification (28). In brief, [^{3}H]colchicine was diluted with ethanol and concentrated by evaporation on a SpeedVac centrifuge for 40 minutes. After centrifugation, [^{3}H]colchicine with or without unlabeled compounds was diluted in binding buffer [1 mmol/L GTP, 1 mmol/L EGTA, 1 mmol/L $MgCl_2$, and 80 mmol/L PIPES (pH 6.8)], and the buffer was subsequently transferred into a 96-well plate (90 μL per well). After transfer, 0.5 μg of biotin-labeled tubulin prepared in 10 μL of binding buffer was added. The total reaction buffer volume was 100 μL/well, and the final concentration of [^{3}H]colchicine was indicated in figure legends. The plates were incubated for 2 hours at 37°C with gentle shaking. After incubation, 0.08 mg of SPA beads in 20 μL of binding buffer was added. After further incubation for 10 minutes under agitation at 37°C, the SPA beads were allowed to settle for 1 hour. A TopCount microplate scintillation counter (PACKARD) was used to perform scintillation counting.

Structural modeling of tivantinib and tubulin by genetic optimization for ligand docking

We predicted the binding poses of tivantinib for the colchicine binding site of tubulin using docking software GOLD version 5.1. The docking score was calculated by GOLD version 5.1. Higher genetic optimization for ligand docking (GOLD) scores correspond to better pose ranks. The X-ray crystal structure of tubulin in a complex with colchicine (PDB code: 1SA0) was used as the initial structure. The statistics program package R was used to perform clustering of 50 tivantinib structures.

Survival assays

Cell survival assay was performed as described previously (11). In brief, 3,000 cells were seeded into 96-well plates in triplet or sextuplet. On the following day, the cells were incubated with the indicated drugs for 72 hours. Cell viability was determined by adding the CellTiter-Glo assay reagent (Promega) for 10 minutes, and using a TriStar LB 941 Multimode Microplate Reader (Berthold Technologies). GraphPad Prism version 5.0 (GraphPad Software) was used to graphically display the data and to determine IC_{50} values.

Apoptosis assay

A total of 1×10^5 cells were seeded into 6-well plates. On the following day, the cells were treated with the indicated concentrations of drugs and incubated for another 72 hours. After incubation, the cells were collected and stained with FITC-labeled Annexin V and 1 μg/mL propidium iodide (PI) for 10 minutes. A Cytomics 500 flow cytometer (Beckman Coulter) was used to assay the cells, and FlowJo software (Tree Star) was used to analyze the data.

Published OnlineFirst October 13, 2014; DOI: 10.1158/1535-7163.MCT-14-0462

Results

Tivantinib inhibits tubulin polymerization and induces G_2–M cell-cycle arrest independent of c-MET inhibition

Previously, we reported that tivantinib disrupts microtubule assembly *in vitro* and *in vivo* (11). However, detailed mechanism underlying inhibition of tubulin polymerization by tivantinib and whether tivantinib shows antitumor activity by microtubule depolymerization were not known.

Because drugs that disrupt microtubules induce aberrant mitotic phenotypes, it is expected that the influence of tivantinib on the cell cycle would be different from other c-MET inhibitors. To monitor the cell cycle in real time, we established Fucci-expressing EBC-1 or SK-MEL-28 cells and observed the cell-cycle progression after treatment with tivantinib or crizotinib. In the Fucci system, human Cdt1 deletion mutants were fused to red fluorescent protein mKO2 (monomeric Kusabira Orange 2), and the N-terminus of human geminin was fused to green fluorescent protein mAG1 (monomeric Azami Green 1). Because Cdt1, a substrate of SCF^{Skp2} complex, expression is highest during G_1 and geminin, a substrate of APC^{cdh1} complex, expression is highest during S–G_2–M phases, Fucci-

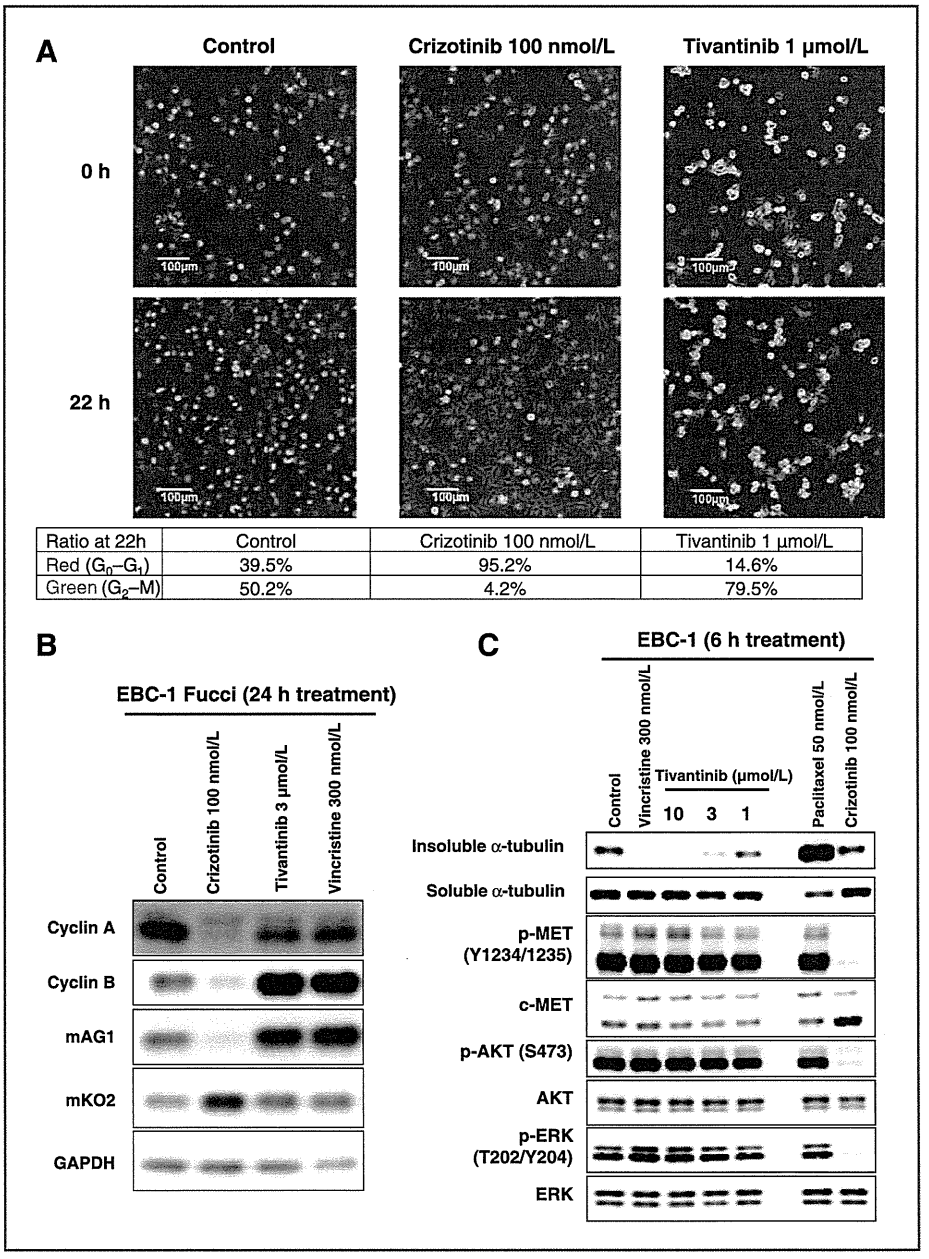

Ratio at 22h	Control	Crizotinib 100 nmol/L	Tivantinib 1 μmol/L
Red (G_0–G_1)	39.5%	95.2%	14.6%
Green (G_2–M)	50.2%	4.2%	79.5%

Figure 1. Tivantinib shows effects different from those of another c-MET inhibitor, crizotinib. A, tivantinib induces G_2–M arrest (green), whereas crizotinib induces G_1 arrest (red) in Fucci-induced EBC-1 cells. Fucci-induced EBC-1 cells were cultured with the indicated concentration of tivantinib and crizotinib for 22 hours. Cell cycles were monitored by time-lapse fluorescence microscopy. Shown are photographs taken at time zero and 22 hours after treatment with each drug. White scale bars indicate 100 μm. Table below indicates the ratio of red fluorescent (G_1 arrest) or green fluorescent (G_2–M) cells measured by flow cytometry 22 hours after treatment with each drug. B, cells were cultured with the indicated concentrations of drugs for 24 hours. Cell lysates were immunoblotted with the indicated antibodies. C, tivantinib inhibits microtubule polymerization but does not inhibit c-MET phosphorylation. EBC-1 cells were treated with 50 nmol/L paclitaxel, 300 nmol/L vincristine, or various concentrations of tivantinib. After the cells were cultured for 6 hours (B), they were lysed with NP-40 lysis buffer and centrifuged at 15,000 *g*; subsequently, the insoluble pellets were lysed in Laemmli Sample Buffer. Both soluble and insoluble lysates were electrophoresed and immunoblotted with the indicated antibodies.

Published OnlineFirst October 13, 2014; DOI: 10.1158/1535-7163.MCT-14-0462

expressing cells emit red light when the cells are in G_1 phase and emit green fluorescence when the cells are in S–G_2–M phase (25). EBC-1 cells are reported as c-MET–addicted cells because of *c-MET* amplification, and SK-MEL-28 cells are known to have *BRAF* mutation and barely express c-MET (Supplementary Fig. S1; refs. 11, 29). After exposure to tivantinib, EBC-1 cells induced G_2–M cell-cycle arrest, whereas crizotinib induced G_0–G_1 arrest (Fig. 1A; Supplementary Fig. S2A; Supplementary Movies 1–3). Consistent with the report that microtubule inhibitors induce metaphase arrest (30), tivantinib treatment reduced cyclin A (which is required for S phase entry) and markedly upregulated cyclin B (which functions in late M phase). Furthermore, crizotinib treatment decreased both cyclin A and B, suggesting the accumulation of G_0–G_1-phase cells (Fig. 1B). In addition, Fucci-expressing SK-MEL-28 cells also showed G_2–M cell-cycle arrest after 3 μmol/L tivantinib treatment, similar to the behavior of the cells treated with 30 nmol/L of vincristine (Supplementary Fig. S2B and S2C; Supplementary Movies 4–6). To quantify the G_0–G_1-phase cells and G_2–M-phase cells, we counted the ratio of the cells emit red or green fluorescence. Consistent with the previous result, tivantinib treatment increased G_2–M-phase cells.

To further clarify the effect of tivantinib on microtubule dynamics, we examined the microtubule assembly state in the cells treated with tivantinib or other drugs. First, *c-MET*–amplified lung cancer EBC-1 cells were treated with 1 μmol/L tivantinib or 100 nmol/L of crizotinib, anaplastic lymphoma receptor tyrosine kinase (ALK) and c-MET inhibitor, for 16 hours and subsequently immunostained with anti–α-tubulin antibody. The tivantinib-treated cells showed cellular microtubule depolymerization with short microtubules in the cytoplasm, whereas the microtubules in the crizotinib-treated cells were not affected (Supplementary Fig. S3). Second, GFP α-tubulin–expressing *KRAS*-mutant lung cancer A549 cells or melanoma SK-MEL-28 cells were treated with tivantinib and observed by time-lapse confocal microscopy. Tivantinib treatment caused disruption of microtubules within 30 minutes (Supplementary Fig. S4).

These results suggest that tivantinib inhibits tubulin polymerization and induces G_2–M cell-cycle arrest independent of c-MET inhibition.

Tivantinib inhibited tubulin polymerization in cells

In our previous study, we performed an *in vitro* tubulin polymerization assay and observed that tivantinib inhibited tubulin polymerization in a dose-dependent manner similar to that by vincristine (11). To determine if tivantinib inhibited tubulin polymerization in cells, we quantified assembled microtubules in cells after tivantinib, paclitaxel, vincristine, or crizotinib treatment. As previously reported, 6-hour paclitaxel treatment significantly increased polymerized tubulin in EBC-1 cells. In contrast, vincristine treatment decreased assembled microtubules (31). As expected, tivantinib treatment inhibited tubulin polymerization in a concentration-dependent manner similar to that by vincristine treatment but surprisingly did not inhibit c-MET and its downstream AKT and ERK signaling pathways. On the other hand, crizotinib treatment did not affect tubulin polymerization but significantly suppressed phosphorylation of c-MET, AKT, and ERK (Fig. 1C). After 24-hour treatment, tivantinib still inhibited tubulin polymerization (Supplementary Fig. S5A). To confirm whether the reduction of polymerized tubulin was independent of c-MET activity, we used c-MET non-addicted H460 cells which expressed c-MET and had weak activity. In previous report, we showed H460 cells were unaffected by knockdown of c-MET (11). Equally to EBC-1 cells, tivantinib treatment inhibited tubulin polymerization dose-dependently in H460 cells (Supplementary Fig. S5B). It was recently reported that tivantinib induced microtubule stabilization in colon cancer DLD-1 cells when the cells were treated with a lower concentration of tivantinib (13). To see if tivantinib would similarly affect DLD-1 cells, we treated DLD-1 cells and quantified the amount of assembled microtubules. Similar to EBC-1 cells, the DLD-1 cells treated with tivantinib also showed a decrease in assembled microtubules in a dose-dependent manner (Supplementary Fig. S5C). These results suggest that tivantinib disrupts microtubule assembly and inhibits tubulin polymerization in cells without regard to c-MET activity.

Tivantinib showed antitumor activity by affecting microtubules

From the results of phase I clinical trials, the mean C_{max} in plasma from patients treated with tivantinib was approximately 5 μmol/L (5, 32–34). After confirming that <5 μmol/L tivantinib induced reduction of polymerized tubulin in cells, we assessed the effect of tivantinib on xenografted human tumors in mice to see if tivantinib inhibited tubulin polymerization *in vivo*. Tivantinib showed antitumor effects at doses of 200 mg/kg twice per day for 5 consecutive days, followed by a 2-day dosing holiday (Fig. 2A). Following this dosing regimen, tivantinib did not show serious side effects, such as body weight loss (Supplementary Fig. S6A). After 19 days of drug treatment, the tumor xenografts were resected from nude mice. The resected tumors were minced, homogenized, and subsequently lysed with tubulin detection buffer according to the same method as used in the experiment with cultured cells. The tivantinib-treated tumors showed significant decreases in tubulin polymerization (insoluble α-tubulin) compared with the levels in the control tumors (Fig. 2B). Furthermore, tivantinib-treated tumor xenografts of the H460 cells also showed antitumor activity and reduction of polymerized tubulin (Fig. 2C and D and Supplementary Fig. S6B). In addition, tivantinib did not induce obvious change on c-MET and GSK-3 status (Supplementary Fig. S6C and S6D). These results suggest that tivantinib exhibits the antitumor effect and disrupting

Published OnlineFirst October 13, 2014; DOI: 10.1158/1535-7163.MCT-14-0462

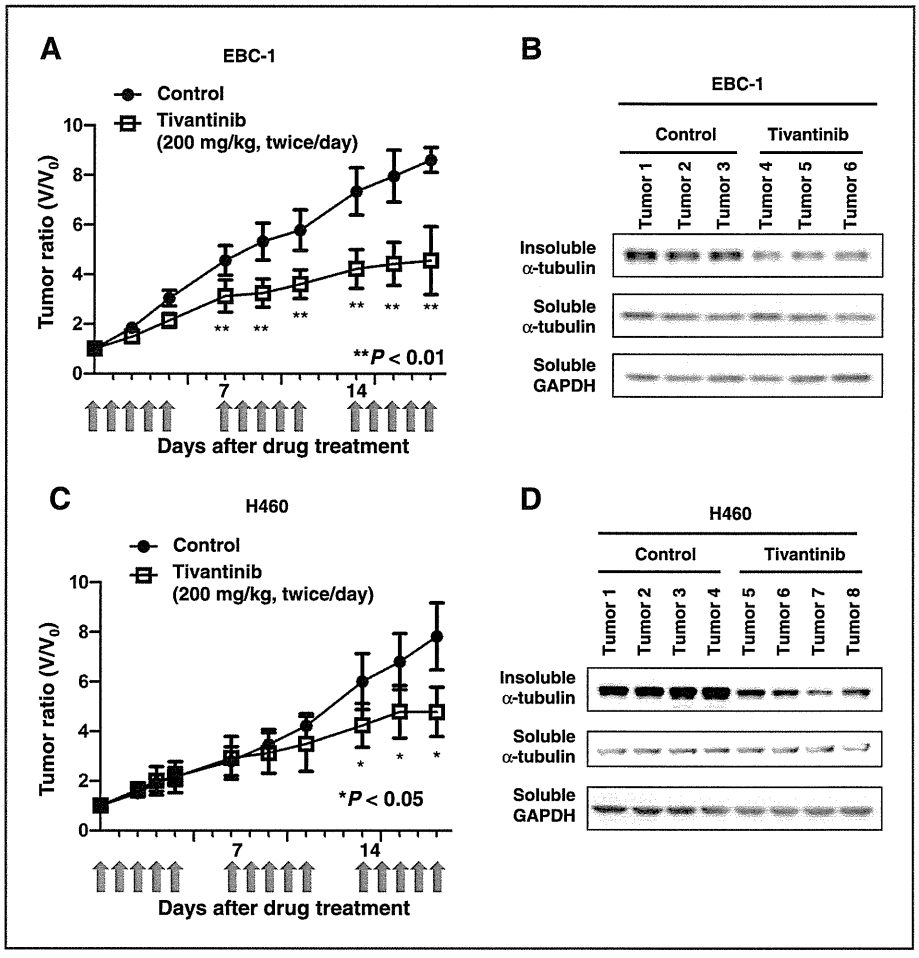

Figure 2. Tivantinib inhibits tumor growth and affects microtubule assembly *in vivo*. A and C, nude mice bearing human lung cancer EBC-1 (A) or H460 (C) cells were treated orally with tivantinib or vehicle control. Drug treatment was started from 5 days after inoculation. Tivantinib was administered at 200 mg/kg twice per day for 5 consecutive days, followed by a 2-day dosing holiday. Data are represented by the mean ± SDs of relative tumor size (standardized by the tumor size at day 0) at each time point ($n = 6$). *, $P < 0.05$ and **, $P < 0.01$ (Mann–Whitney U test) for the tivantinib-treated mice compared with that for the controls. B and D, tumors of EBC-1 (B) or H460 (D) resected from nude mice 19 days after drug treatment and homogenized with lysis buffer. Cell lysates were filtered through a 0.80-μm filter and subsequently immunoblotted according to the same protocol as used in Figure 1. Each tumor (tumors 1, 2, and 3) was resected from a different mouse.

microtubule assembly *in vivo* as well as *in vitro* independent of c-MET status.

Tivantinib directly binds to tubulin at colchicine binding site

It is well known that microtubule-destabilizing agents, such as vincristine and colchicine, directly bind to tubulins at several different binding sites (35, 36). To determine if tivantinib directly binds to tubulin in a manner similar to that by other microtubule inhibitors, we estimated the effect of tivantinib or other small-molecule inhibitors on [^{3}H]colchicine binding to tubulin using a competition binding SPA. Interestingly, tivantinib inhibited [^{3}H]colchicine binding to tubulin in a dose-dependent manner similar to that by unlabeled colchicine (Fig. 3A). As expected, vincristine, vinblastine, and crizotinib did not affect [^{3}H]colchicine binding to tubulin. To determine if tivantinib interferes with the tubulin binding of vincristine or vinblastine, which have been shown to bind to the vinca domain of tubulin, DEAE-cellulose filters were used to test the effect of tivantinib on [^{3}H]vincristine or [^{3}H]vinblastine binding to tubulin. As expected, unlabeled vincristine and vinblastine, but not tivantinib, colchicine, or crizotinib, inhibited both [^{3}H]vincristine and [^{3}H]vinblastine binding to tubulin (Supplementary Fig. S7A and S7B). These results suggest that tivantinib affects colchicine–tubulin binding. To determine if tivantinib competitively or noncompetitively inhibits colchicine binding to tubulin, we performed a binding assay with increasing concentrations of [^{3}H]colchicine in the presence of tivantinib and calculated the B_{max} and Kd values for colchicine binding to tubulin using nonlinear regression analysis. Consistent with the increase in tivantinib concentration, the Kd values for colchicine but not for B_{max} binding to tubulin increased (Fig. 3B). These results suggest that tivantinib directly interacts with tubulin via the colchicine binding site, and competitively inhibits colchicine binding to tubulin.

On the basis of these *in vitro* results, we perform a computational simulation of the binding model in which tivantinib binds to the colchicine binding site of tubulin using GOLD docking program. In this study, we used the well-known tubulin–colchicine structure reported by Ravelli and colleagues (35). To validate the GOLD simulation findings, we pulled colchicine out of the binding site and consequently redocked colchicine into the structure.

Published OnlineFirst October 13, 2014; DOI: 10.1158/1535-7163.MCT-14-0462

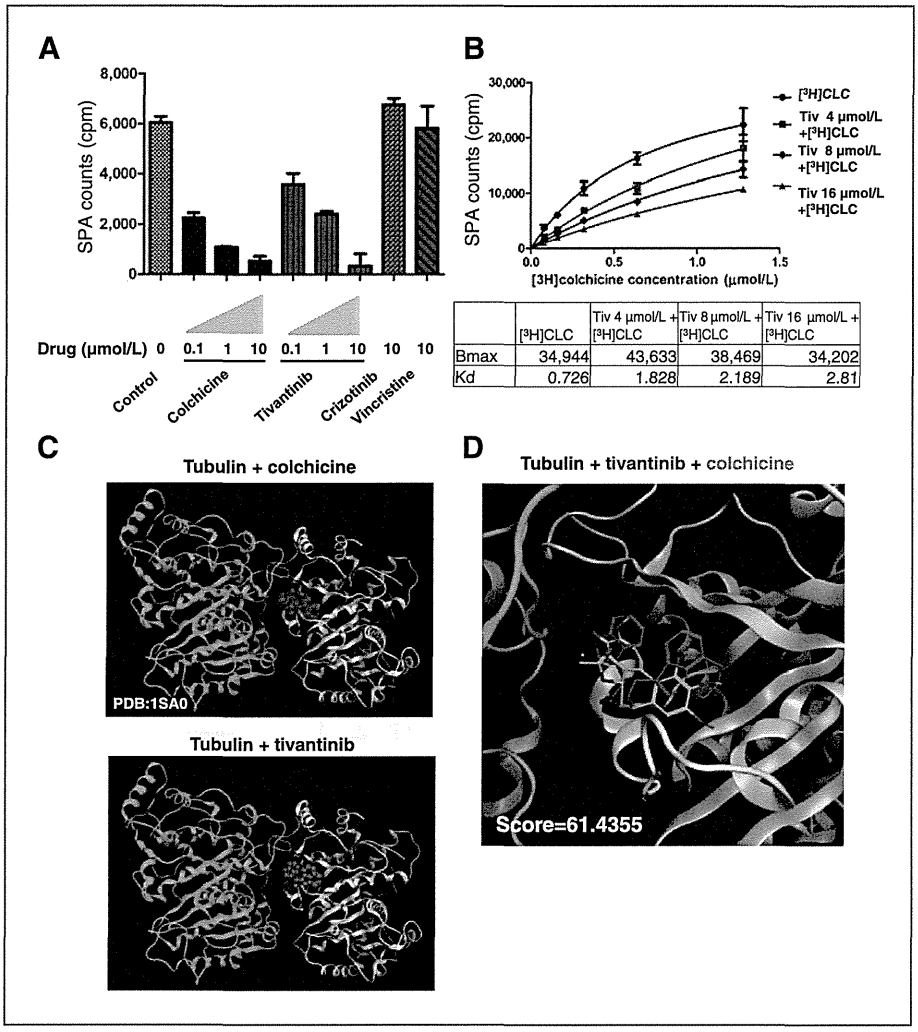

	[3H]CLC	Tiv 4 μmol/L + [3H]CLC	Tiv 8 μmol/L + [3H]CLC	Tiv 16 μmol/L + [3H]CLC
Bmax	34,944	43,633	38,469	34,202
Kd	0.726	1.828	2.189	2.81

Figure 3. Analysis of binding modes of tivantinib with tubulin. A, competition assay of various small-molecule inhibitors, including tivantinib with [^{3}H]colchicine, for binding to purified tubulin. Biotin-labeled tubulin was incubated with 0.3 μmol/L [^{3}H]colchicine and the indicated concentration of each compound at 37°C for 2 hours. After incubation, the binding of [^{3}H]colchicine to tubulin was quantified by scintillation proximity assay. Each data point represents the mean ± SD. B, tivantinib shows competitive inhibition of colchicine–tubulin binding. The following concentrations of [^{3}H]colchicine ([^{3}H]CLC) were incubated with the indicated concentrations of tivantinib (0.08, 0.16, 0.32, 0.64, and 1.28 μmol/L each). Graphpad Prism was used to perform nonlinear regression analysis to calculate the B_{max} and Kd for colchicine–tubulin binding. Data are represented by the mean ± SD. In this figure, "Tiv" indicates tivantinib and "CLC" indicates colchicine. C, structure model of tubulin–DAMA colchicine (red) was drawn with PyMOL software using a reported crystal structure data (PDB ID: 1sa0; top). The GOLD docking program was used to calculate the predicted binding structure model of tubulin–tivantinib (blue), which was illustrated using PyMOL software (bottom). D, shown is an overlay of colchicine (cyan) and tivantinib (magenta) on tubulin. The top-ranked docking pose of tivantinib with tubulin on the tubulin–colchicine binding model is shown.

The top-ranked tubulin–colchicine structure simulated by the GOLD program showed a conformation quite similar to that of the original crystal structure. Next, we extracted colchicine from the reported structure and docked tivantinib (Fig. 3C). In this docking study, the top 50 structures calculated by the GOLD program were clustered into 10 groups (Fig. 3D and Supplementary Fig. S8). As shown in Fig. 3D, the top-scored tivantinib molecule was highly overlapped with the colchicine molecule in the binding pocket of tubulin. These results predict that tivantinib directly binds to the colchicine site of tubulin without steric hindrance.

Tivantinib showed cytotoxic activity against tubulin binder-resistant cells

The microtubule inhibitors, paclitaxel, vincristine, and vinblastine, are commonly used in the treatment of various cancers, but development of acquired resistance can prevent success. For example, overexpression of the drug efflux pump is one major mechanism of drug resistance. To determine if tivantinib could overcome drug resistance, we tested the cytotoxic activity of tivantinib against tubulin binding agent-resistant cells. In this assay, we used clones of K562 and CEM cells that showed acquired resistance to vinca alkaloid. These resistant clones of

Published OnlineFirst October 13, 2014; DOI: 10.1158/1535-7163.MCT-14-0462

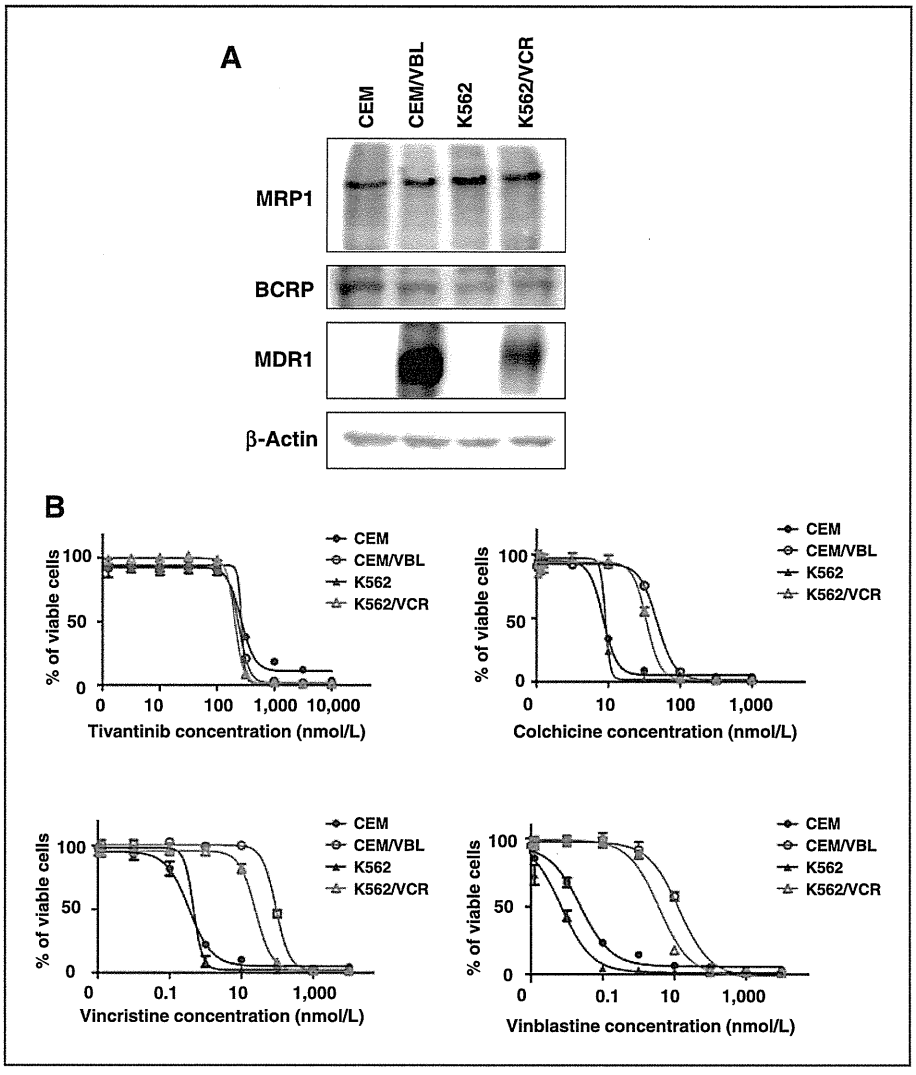

Figure 4. The effect of tivantinib on vinca alkaloid–resistant cells. A, the expression of ABC transporters. Cells were cultured with the indicated concentrations of drugs for 24 hours. Cell lysates were immunoblotted with the indicated antibodies (B). K562 VCR, K562, CCRF-CEM, and CEM/VBL cells were treated with the indicated concentrations of tivantinib (top left), colchicine (top right), vincristine (bottom left), or vinblastine (bottom right) for 72 hours. Cell viability was assessed by CellTiter-Glo assay. Error bars show the SDs; $n = 3$. Repeated experiments gave similar results.

K562/VCR and CEM/VBL were obtained by growing the cells in the presence of sublethal concentrations of drug, and the cells were shown to acquire resistance by overexpressing MDR1 (23, 24; Fig. 4A). As expected, K562/VCR or CEM/VBL cells showed cross-resistance to vinblastine, vincristine, or colchicine, but surprisingly, these microtubule inhibitor–resistant cells were still sensitive to tivantinib (Fig. 4B).

Tivantinib overcomes drug resistance mediated by major ABC transporters

Next, we examined the sensitivity of tivantinib in KB3-1 cells that overexpressed various ABC transporters (Fig. 5A; ref. 37). Ectopic overexpression of MDR1 resulted in acquired resistance to vincristine and slight resistance to adriamycin in KB3-1 cells. In addition, BCRP-overexpressed KB3-1 cells exhibited resistance to SN-38, and MRP1 overexpression resulted in resistance to adriamycin and slightly to vincristine (38). To our surprise, tivantinib showed the same cytotoxic activity in these ABC transporter–overexpressing cells (Fig. 5B). Next, we used PI and FITC-labeled Annexin V staining to measure induction of apoptosis. Consistent with the results from a cell viability assay, MDR1-overexpressing KB3-1 cells acquired resistance to vincristine, but all of the cells similarly induced apoptosis after tivantinib treatment (Fig. 6A and Supplementary Fig. S9A). Because of the fluorescence of SN-38 or adriamycin, we could not assess the apoptosis by FITC-Annexin V/PI staining. Therefore, we measured apoptotic cells by sub-G_1 analysis. As expected, we observed that KB3-1 cells that overexpressed BCRP did not undergo apoptosis by SN-38 treatment and KB3-1 cells that overexpressed MRP1 did not increase apoptosis by adriamycin (Supplementary Fig. S9B). After 24-hour treatment with tivantinib, cleaved PARP expression was equally induced in all of the cells, whereas vincristine did not induce PARP cleavage in the MDR1-overexpressed cells, SN-38 did not induce PARP cleavage

Published OnlineFirst October 13, 2014; DOI: 10.1158/1535-7163.MCT-14-0462

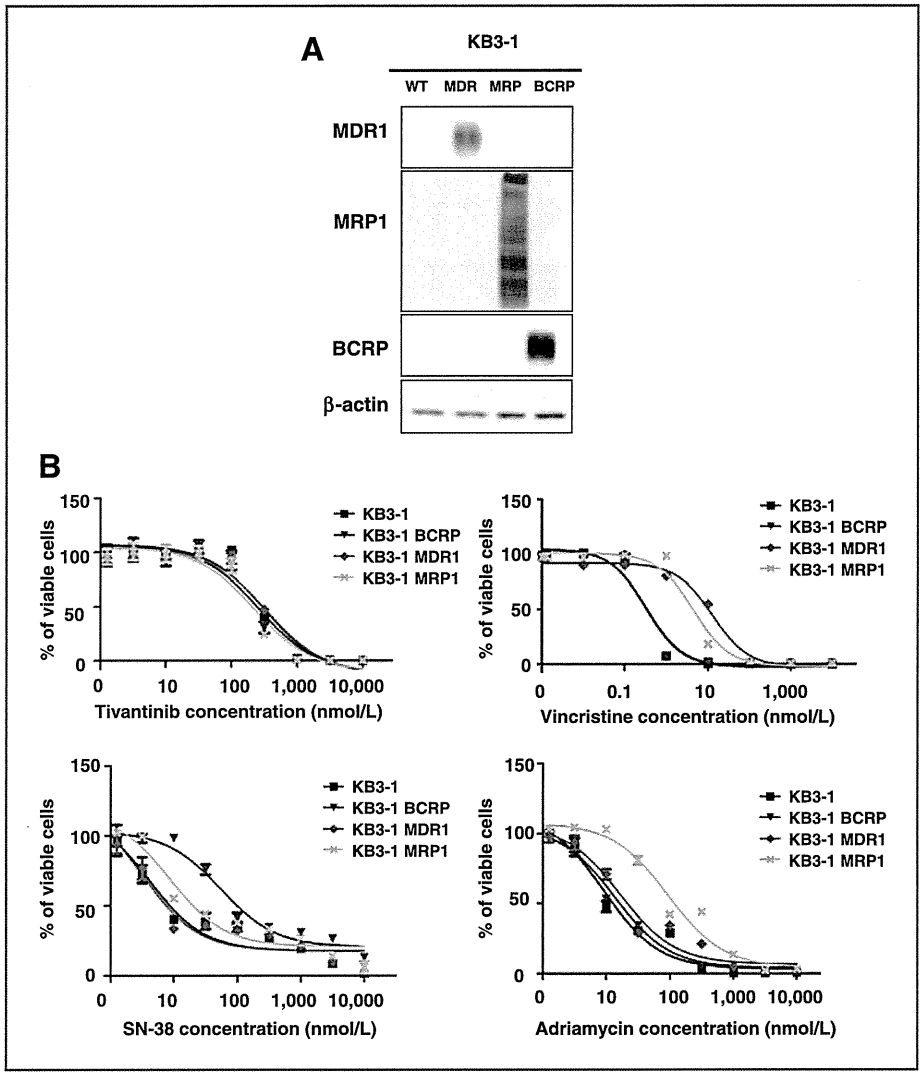

Figure 5. The effect of tivantinib on various cells overexpressing ABC transporters. In this figure, MDR1-overexpressed KB3-1 cells are indicated as "KB3-1 MDR1"; similarly, MRP1- or BCRP-overexpressed cells are indicated as "KB3-1 MRP1" or "KB3-1 BCRP," respectively. A, the expression of ABC transporters. Cells were cultured with the indicated concentrations of drugs for 24 hours. Cell lysates were immunoblotted with the indicated antibodies. B, MDR1-, MRP1-, or BCRP-overexpressed KB3-1 cells and parental KB3-1cells were treated with the indicated concentrations of tivantinib (top left), vincristine (top right), SN-38 (bottom left), or adriamycin (bottom right) for 72 hours. Cell viability was assessed by CellTiter-Glo assay. Error bars show the SDs; $n = 6$.

in BCRP-overexpressed cells, and adriamycin did not induce PARP cleavage in MRP1-overexpressed cells (Fig. 6B).

Discussion

Tivantinib was first reported as a highly selective inhibitor of c-MET and is currently being investigated in a phase III clinical trial based on the result of early clinical trials that increased OS and PFS in MET-high population (3, 6, 8). Because c-MET activation by *c-MET* gene amplification or HGF upregulation is related to acquired resistance to EGFR-TKI, a phase II study of EGFR-TKI erlotinib with or without tivantinib treatment for patients with advanced NSCLC was initiated. Although that study did not meet the primary endpoint, a small cohort of patients with *KRAS* mutations significantly improved PFS in the tivantinib combined with erlotinib-treated patients (7). This result is surprising because KRAS is downstream of c-MET, and *KRAS*-mutated cells have been reported to be insensitive to other c-MET inhibitors, such as PHA-665752 and crizotinib (9, 13). To explain these inconsistencies, we and Basilico and colleagues recently showed that tivantinib inhibited cell proliferation independent of addiction to c-MET and disrupted microtubule dynamics (11, 13, 14). Considering that tivantinib is currently in a phase III clinical trial and has shown encouraging antitumor activity, it is very important to clarify the true target of tivantinib. To investigate the mechanism underlying how tivantinib affects cell growth, we first used Fucci-expressing cells to compare the effect of tivantinib on cell cycling. The tivantinib-treated cells primarily emitted green fluorescence, which showed that tivantinib treatment induced G_2–M arrest and that the treatment with the potent c-MET/ALK inhibitor, crizotinib, induced G_1 arrest (Fig. 1A and B and

Published OnlineFirst October 13, 2014; DOI: 10.1158/1535-7163.MCT-14-0462

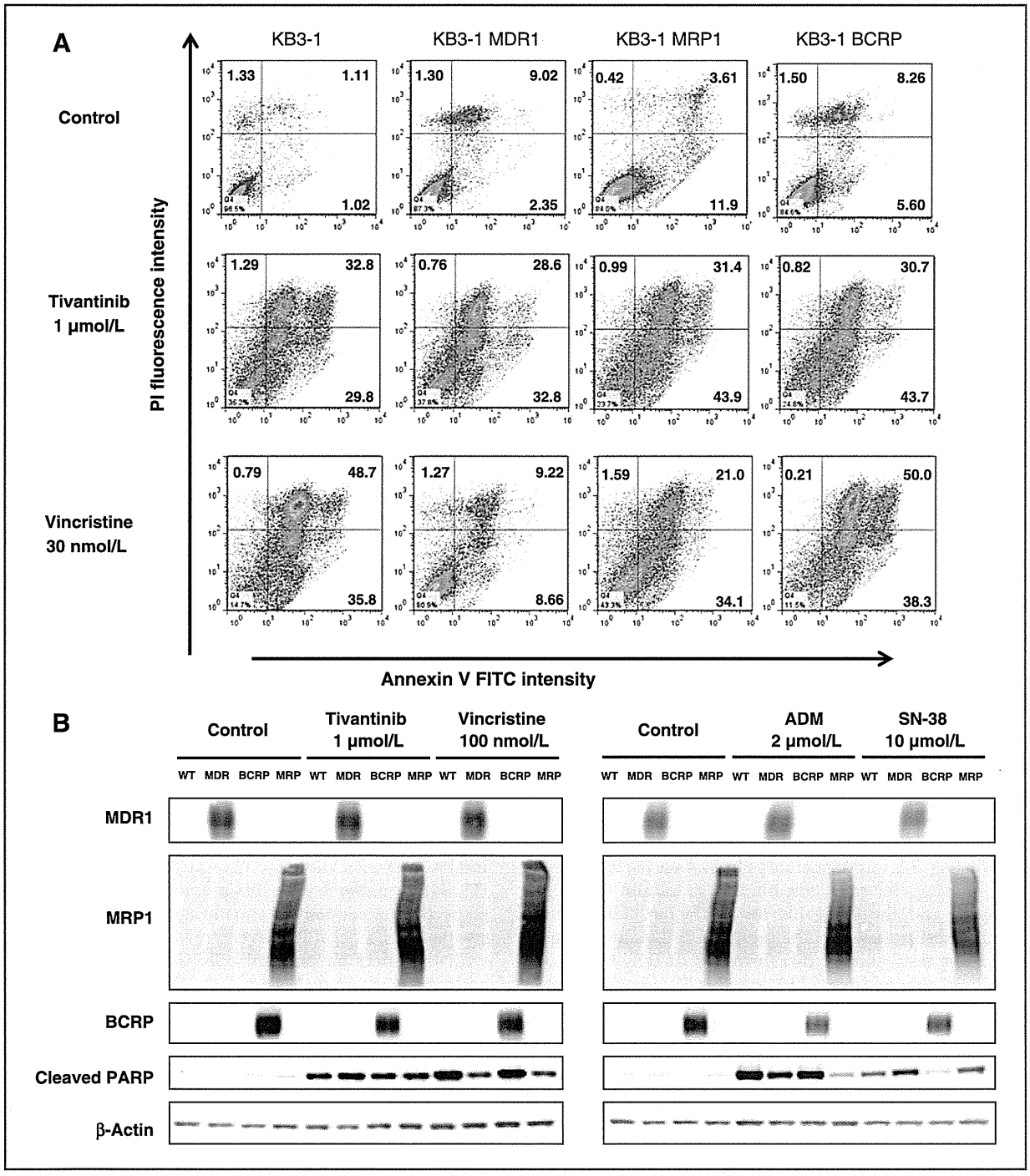

Figure 6. Tivantinib induces apoptosis in cells overexpressing various ABC transporters. A, flow cytometry analyses of apoptotic cells. Cells were treated with the indicated concentrations of SN-38, adriamycin, vincristine, or tivantinib for 72 hours. After 72 hours, tivantinib- or vincristine-treated cells were stained with PI and FITC-labeled Annexin V and analyzed on a FC 500 flow cytometer. B, expression of cleaved PARP and ABC transporters. Cells were cultured with the indicated concentrations of drugs for 24 hours. Cell lysates were immunoblotted with the indicated antibodies.

Supplementary Fig. S2A–S2C). It has been reported that treatment with microtubule inhibitors, such as vincristine or paclitaxel, induced G_2–M arrest in cancer cells, and cells treated with tyrosine kinase inhibitors, such as erlotinib or gefitinib, often showed G_1 arrest in various *EGFR*-mutated NSCLC cell lines (39, 40). Consistent

Published OnlineFirst October 13, 2014; DOI: 10.1158/1535-7163.MCT-14-0462

with our previous report, these results indicate that the mode of action of tivantinib is different from that of other tyrosine kinase inhibitors (11).

To clarify the effect of tivantinib on microtubule status in cells and *in vivo*, we quantified polymerized tubulin after tivantinib treatment. In EBC-1 cells, tivantinib decreased polymerized tubulin in a dose-dependent manner (Fig. 1C). Moreover, at this concentration of tivantinib, c-MET and downstream AKT/ERK were not inhibited. From the phase I dose-escalation study, the reported C_{max} of tivantinib was approximately 5 μmol/L (5, 32–34). Because we confirmed that <5 μmol/L tivantinib could inhibit tubulin polymerization in EBC-1 cells, we determined if tivantinib also could inhibit tubulin polymerization *in vivo*. Similar to the *in vitro* study results, tumor xenografts of tivantinib-treated mice showed reduction of polymerized tubulin compared with the level in the controls (Fig. 2B and D). This result suggests that the antitumor effect of tivantinib is associated with tubulin polymerization inhibition. Previous confocal analysis suggested that treatment with several hundred nanomolar concentrations of tivantinib induced microtubule stabilization in DLD-1 cell (13). To determine if tivantinib inhibited tubulin polymerization in DLD-1 cells, we measured cellular polymerized tubulin and confirmed that tivantinib reduced tubulin polymerization at an approximate 3 μmol/L concentration, which is lower than the C_{max} of tivantinib (Supplementary Fig. S5C). These results again suggested that tivantinib impairs microtubules by inhibiting tubulin polymerization.

Most tubulin-targeting drugs are known to directly bind to β-tubulin at three different sites, such as the vinca binding site, taxane binding site, or colchicine binding site (36). In this study, we showed that tivantinib dose-dependently inhibited [^{3}H]colchicine binding to tubulin and did not affect [^{3}H]vincristine or [^{3}H]vinblastine binding to tubulin (Fig. 3A; Supplementary Fig. S7A and S7B). Moreover, the B_{max} for colchicine binding to tubulin was not changed, and the Kd value for colchicine binding to tubulin was increased in the presence of tivantinib (Fig. 3B). These results imply that tivantinib directly binds to tubulin at the colchicine binding site. It is known that classical tubulin inhibitors, such as paclitaxel and vincristine, produce a painful peripheral neuropathy; however, previous clinical trials have shown that there is no neurotoxicity at all in patients treated with tivantinib. This finding of minimal neuropathy is similar to that for recently approved tubulin-targeted inhibitors, such as eribulin and the semi-synthetic vinca alkaloid, vinflunine, for which the incidence of peripheral neuropathy was lower than those for paclitaxel or vinblastine. In addition, the Ki value of tivantinib was calculated to be approximately 9 μmol/L by using the Cheng–Prusoff equation, and the Ki value was lower than those of other colchicine-site binding agents previously reported (28), which suggests that tivantinib might have a slightly weak effect on tubulin polymerization. However, vinflunine is known to have less affinity for the vinca binding site of tubulin than does vincristine in mouse models and to show a potent antitumor effect with lower neurotoxicity in clinical trials (41, 42). The mechanism of microtubule inhibition by vinflunine has been reported to involve increase of microtubule growth duration and suppression of the treadmilling rate, but the effects were weaker than vinblastine. In addition, vinflunine has been reported to induce reduction of the microtubule growth rate (43). On the other hand, the molecular mechanism underlying how tivantinib inhibits microtubules remains unknown. Moreover, Remsing Rix and colleagues (16) recently reported that GSK3α and GSK3β are new target kinases of tivantinib. Further study is needed to elucidate the mechanism in detail.

Consistent with the results of the tubulin binding competition assay, computational prediction of tubulin–tivantinib binding also suggested that tivantinib directly binds to the colchicine site of tubulin without steric hindrance (Fig. 3C and D). However, because the resolution of the reported tubulin–DAMA colchicine structure was low, the predicted model of tivantinib–tubulin has a higher degree of uncertainty. Further experiments would be required to elucidate the binding mode of tivantinib.

Microtubule-targeting agents have been widely used in cancer chemotherapy; however, the emergence of resistant tumors is a major obstacle. As one of the resistant mechanisms to microtubule-targeting drugs, MDR1 overexpression was identified in various cancer cells (18). MDR1 is one of the ABC transporter proteins that confers resistance by pumping out various microtubule inhibitors, such as colchicine, taxol, and vincristine. In our previous report, the result of a COMPARE analysis involving *in silico* screening of a database of drug sensitivities across 39 cancer cell lines showed that tivantinib exhibited similar IC_{50} values across 39 cancer cells including HCT-15 cells known to naturally overexpress MDR1 (11, 44). Consistent with this previous result, tivantinib showed cytotoxic activity equally against vinca alkaloid–resistant cells or MDR1-overexpressed cells compared with the effect on parental cells (Figs. 4B and 5B). In addition, it is widely known that other ABC transporter BCRP confers resistance to topotecan and that MRP1 confers resistance to adriamycin. Tivantinib equally inhibited growth of cells overexpressing BCRP or MRP1 (Figs. 5B and 6A and B).

In clinical trials, tivantinib showed encouraging antitumor activity and was well tolerated. However, the additional possible targets of tivantinib were unknown. In this study, we showed that tivantinib inhibited tubulin polymerization in cells and tumors. Moreover, we suggest that tivantinib directly interacts with tubulin at the colchicine binding site and overcomes the effects of drug resistance–mediating ABC transporters. However, the detailed mechanism underlying inhibition of tubulin polymerization by tivantinib remains unknown. Moreover, it is expected that cells may acquire resistance to tivantinib in a manner similar to that for other

Published OnlineFirst October 13, 2014; DOI: 10.1158/1535-7163.MCT-14-0462

drugs. However, the mechanism of acquired resistance to tivantinib remains unknown. Currently, tivantinib is under clinical evaluation as a selective c-MET inhibitor and showed lower toxicity. Our finding that tivantinib shows cytotoxic activity by disrupting tubulin polymerization, directly interacts with tubulin, and overcomes ABC transporter–mediated drug resistance suggests that tivantinib may be useful for treatment of a variety of other cancers.

Disclosure of Potential Conflicts of Interest

No potential conflicts of interest were disclosed.

Authors' Contributions

Conception and design: A. Aoyama, R. Katayama, N. Fujita
Development of methodology: A. Aoyama, R. Katayama, N. Fujita
Acquisition of data (provided animals, acquired and managed patients, provided facilities, etc.): A. Aoyama, R. Katayama, T. Oh-hara, S. Sato
Analysis and interpretation of data (e.g., statistical analysis, biostatistics, computational analysis): A. Aoyama, R. Katayama, T. Oh-hara, S. Sato, Y. Okuno, N. Fujita
Writing, review, and/or revision of the manuscript: A. Aoyama, R. Katayama, Y. Okuno, N. Fujita
Administrative, technical, or material support (i.e., reporting or organizing data, constructing databases): A. Aoyama, T. Oh-hara, S. Sato, N. Fujita
Study supervision: R. Katayama, N. Fujita

Acknowledgments

The authors thank Ms. Sumie Koike for helping with data analysis and Drs. Atsushi Miyawaki and Hiroyuki Miyoshi, RIKEN, for providing the CSII-EF-MCS vectors encoding mCherry-hCdt1 and mVenus-hGem.

Grant Support

The study was supported in part by Japan Society for the Promotion of Science KAKENHI grant numbers 24300344 and 22112008 (to N. Fujita) and 25710015 (to R. Katayama) and a research grant of the Princess Takamatsu Cancer Research Fund (to N. Fujita).

Received May 29, 2014; revised September 16, 2014; accepted September 24, 2014; published OnlineFirst October 13, 2014.

References

1. Gherardi E, Birchmeier W, Birchmeier C, Vande Woude G. Targeting MET in cancer: rationale and progress. Nat Rev Cancer 2012;12:89–103.
2. Peters S, Adjei AA. MET: a promising anticancer therapeutic target. Nat Rev Clin Oncol 2012;9:314–26.
3. Munshi N, Jeay S, Li Y, Chen CR, France DS, Ashwell MA, et al. ARQ 197, a novel and selective inhibitor of the human c-Met receptor tyrosine kinase with antitumor activity. Mol Cancer Ther 2010;9:1544–53.
4. Eathiraj S, Palma R, Volckova E, Hirschi M, France DS, Ashwell MA, et al. Discovery of a novel mode of protein kinase inhibition characterized by the mechanism of inhibition of human mesenchymal-epithelial transition factor (c-Met) protein autophosphorylation by ARQ 197. J Biol Chem 2011;286:20666–76.
5. Yap TA, Olmos D, Brunetto AT, Tunariu N, Barriuso J, Riisnaes R, et al. Phase I trial of a selective c-MET inhibitor ARQ 197 incorporating proof of mechanism pharmacodynamic studies. J Clin Oncol 2011;29:1271–9.
6. Rimassa L, Porta C, Borbath I, Daniele B, Finn RS, Raoul J-L, et al. Tivantinib in MET-high hepatocellular carcinoma patients and the ongoing Phase III clinical trial. Hepatic Oncol 2014;1:181–8.
7. Sequist LV, von Pawel J, Garmey EG, Akerley WL, Brugger W, Ferrari D, et al. Randomized phase II study of erlotinib plus tivantinib versus erlotinib plus placebo in previously treated non-small-cell lung cancer. J Clin Oncol 2011;29:3307–15.
8. Scagliotti G, Novello S, Ramlau R, Favaretto A, Barlesi F, Akerley W, et al. A phase III study of tivantinib plus erlotinib did not meet a primary endpoint in patients with locally-advanced or metastatic, non-squamous NSCLC. Eur J Cancer 2013;49.
9. Yasuda H, de Figueiredo-Pontes LL, Kobayashi S, Costa DB. Preclinical rationale for use of the clinically available multitargeted tyrosine kinase inhibitor crizotinib in *ROS1*-translocated lung cancer. J Thorac Oncol 2012;7:1086–90.
10. Smolen GA, Sordella R, Muir B, Mohapatra G, Barmettler A, Archibald H, et al. Amplification of *MET* may identify a subset of cancers with extreme sensitivity to the selective tyrosine kinase inhibitor PHA-665752. Proc Natl Acad Sci U S A 2006;103:2316–21.
11. Katayama R, Aoyama A, Yamori T, Qi J, Oh-hara T, Song Y, et al. Cytotoxic activity of tivantinib (ARQ 197) is not due solely to c-MET inhibition. Cancer Res 2013;73:3087–96.
12. Michieli P, Di Nicolantonio F. Targeted therapies: Tivantinib–a cytotoxic drug in MET inhibitor's clothes? Nat Rev Clin Oncol 2013;10:372–4.
13. Basilico C, Pennacchietti S, Vigna E, Chiriaco C, Arena S, Bardelli A, et al. Tivantinib (ARQ197) displays cytotoxic activity that is independent of its ability to bind MET. Clin Cancer Res 2013;19:2381–92.
14. Rimassa L, Bruix J, Broggini M, Santoro A. Tivantinib (ARQ197) displays cytotoxic activity that is independent of its ability to bind MET–letter. Clin Cancer Res 2013;19:4290.
15. Michieli P, Basilico C, Pennacchietti S. Tivantinib (ARQ197) displays cytotoxic activity that is independent of its ability to bind MET–response. Clin Cancer Res 2013;19:4291.
16. Remsing Rix LL, Kuenzi BM, Luo Y, Remily-Wood E, Kinose F, Wright G, et al. GSK3 alpha and beta are new functionally relevant targets of tivantinib in lung cancer cells. ACS Chem Biol 2013;9:353–8.
17. Chen CJ, Chin JE, Ueda K, Clark DP, Pastan I, Gottesman MM, et al. Internal duplication and homology with bacterial transport proteins in the *mdr1* (P-glycoprotein) gene from multidrug-resistant human cells. Cell 1986;47:381–9.
18. Gottesman MM, Fojo T, Bates SE. Multidrug resistance in cancer: role of ATP-dependent transporters. Nat Rev Cancer 2002;2:48–58.
19. Mozzetti S, Ferlini C, Concolino P, Filippetti F, Raspaglio G, Prislei S, et al. Class III beta-tubulin overexpression is a prominent mechanism of paclitaxel resistance in ovarian cancer patients. Clin Cancer Res 2005;11:298–305.
20. Hari M, Wang Y, Veeraraghavan S, Cabral F. Mutations in alpha- and beta-tubulin that stabilize microtubules and confer resistance to colcemid and vinblastine. Mol Cancer Ther 2003;2:597–605.
21. Vahdat L. Ixabepilone: a novel antineoplastic agent with low susceptibility to multiple tumor resistance mechanisms. Oncologist 2008;13:214–21.
22. Jordan MA, Kamath K, Manna T, Okouneva T, Miller HP, Davis C, et al. The primary antimitotic mechanism of action of the synthetic halichondrin E7389 is suppression of microtubule growth. Mol Cancer Ther 2005;4:1086–95.
23. Beck WT, Mueller TJ, Tanzer LR. Altered surface membrane glycoproteins in Vinca alkaloid-resistant human leukemic lymphoblasts. Cancer Res 1979;39:2070–6.
24. Tsuruo T, Iida H, Tsukagoshi S, Sakurai Y. Potentiation of vincristine and Adriamycin effects in human hemopoietic tumor cell lines by calcium antagonists and calmodulin inhibitors. Cancer Res 1983;43:2267–72.
25. Sakaue-Sawano A, Kurokawa H, Morimura T, Hanyu A, Hama H, Osawa H, et al. Visualizing spatiotemporal dynamics of multicellular cell-cycle progression. Cell 2008;132:487–98.

Published OnlineFirst October 13, 2014; DOI: 10.1158/1535-7163.MCT-14-0462

26. Katayama R, Shaw AT, Khan TM, Mino-Kenudson M, Solomon BJ, Halmos B, et al. Mechanisms of acquired crizotinib resistance in ALK-rearranged lung Cancers. Sci Transl Med 2012;4:120ra17.
27. Blagosklonny MV, Schulte TW, Nguyen P, Mimnaugh EG, Trepel J, Neckers L. Taxol induction of p21WAF1 and p53 requires c-*raf*-1. Cancer Res 1995;55:4623–6.
28. Tahir SK, Kovar P, Rosenberg SH, Ng SC. Rapid colchicine competition-binding scintillation proximity assay using biotin-labeled tubulin. Biotechniques 2000;29:156–60.
29. Davies H, Bignell GR, Cox C, Stephens P, Edkins S, Clegg S, et al. Mutations of the *BRAF* gene in human cancer. Nature 2002;417: 949–54.
30. Jordan MA, Wilson L. Microtubules as a target for anticancer drugs. Nat Rev Cancer 2004;4:253–65.
31. Chang JY, Chang CY, Kuo CC, Chen LT, Wein YS, Kuo YH. Salvinal, a novel microtubule inhibitor isolated from *Salvia miltiorhizae* Bunge (Danshen), with antimitotic activity in multidrug-sensitive and -resistant human tumor cells. Mol Pharmacol 2004;65:77–84.
32. Wagner AJ, Goldberg JM, Dubois SG, Choy E, Rosen L, Pappo A, et al. Tivantinib (ARQ 197), a selective inhibitor of MET, in patients with microphthalmia transcription factor-associated tumors: results of a multicenter phase 2 trial. Cancer 2012;118:5894–902.
33. Rosen LS, Senzer N, Mekhail T, Ganapathi R, Chai F, Savage RE, et al. A phase I dose-escalation study of tivantinib (ARQ 197) in adult patients with metastatic solid tumors. Clin Cancer Res 2011;17: 7754–64.
34. Goldman JW, Laux I, Chai F, Savage RE, Ferrari D, Garmey EG, et al. Phase 1 dose-escalation trial evaluating the combination of the selective MET (mesenchymal-epithelial transition factor) inhibitor tivantinib (ARQ 197) plus erlotinib. Cancer 2012;118:5903–11.
35. Ravelli RB, Gigant B, Curmi PA, Jourdain I, Lachkar S, Sobel A, et al. Insight into tubulin regulation from a complex with colchicine and a stathmin-like domain. Nature 2004;428:198–202.
36. Dumontet C, Jordan MA. Microtubule-binding agents: a dynamic field of cancer therapeutics. Nat Rev Drug Discov 2010;9:790–803.
37. Katayama R, Koike S, Sato S, Sugimoto Y, Tsuruo T, Fujita N. Dofequidar fumarate sensitizes cancer stem-like side population cells to chemotherapeutic drugs by inhibiting ABCG2/BCRP-mediated drug export. Cancer Sci 2009;100:2060–8.
38. Loe DW, Deeley RG, Cole SP. Characterization of vincristine transport by the M(r) 190,000 multidrug resistance protein (MRP): evidence for cotransport with reduced glutathione. Cancer Res 1998;58:5130–6.
39. Ling YH, Li T, Yuan Z, Haigentz M Jr, Weber TK, Perez-Soler R. Erlotinib, an effective epidermal growth factor receptor tyrosine kinase inhibitor, induces p27KIP1 up-regulation and nuclear translocation in association with cell growth inhibition and G1/S phase arrest in human non-small-cell lung cancer cell lines. Mol Pharmacol 2007;72:248–58.
40. Huang SM, Li J, Armstrong EA, Harari PM. Modulation of radiation response and tumor-induced angiogenesis after epidermal growth factor receptor inhibition by ZD1839 (Iressa). Cancer Res 2002;62: 4300–6.
41. Etievant C, Kruczynski A, Barret JM, Tait AS, Kavallaris M, Hill BT. Markedly diminished drug resistance-inducing properties of vinflunine (20′,20′-difluoro-3′,4′-dihydrovinorelbine) relative to vinorelbine, identified in murine and human tumour cells in vivo and in vitro. Cancer Chemother Pharmacol 2001;48:62–70.
42. Schutz FA, Bellmunt J, Rosenberg JE, Choueiri TK. Vinflunine: drug safety evaluation of this novel synthetic vinca alkaloid. Expert Opin Drug Saf 2011;10:645–53.
43. Ngan VK, Bellman K, Panda D, Hill BT, Jordan MA, Wilson L. Novel actions of the antitumor drugs vinflunine and vinorelbine on microtubules. Cancer Res 2000;60:5045–51.
44. Loganzo F, Discafani CM, Annable T, Beyer C, Musto S, Hari M, et al. HTI-286, a synthetic analogue of the tripeptide hemiasterlin, is a potent antimicrotubule agent that circumvents P-glycoprotein-mediated resistance *in vitro* and *in vivo*. Cancer Res 2003;63:1838–45.

Published OnlineFirst September 16, 2014; DOI: 10.1158/1078-0432.CCR-14-1511

Clinical Cancer Research

Personalized Medicine and Imaging

See related commentary by Politi and Gettinger, p. 5576

Two Novel ALK Mutations Mediate Acquired Resistance to the Next-Generation ALK Inhibitor Alectinib

Ryohei Katayama[1,2,3], Luc Friboulet[1,2], Sumie Koike[3], Elizabeth L. Lockerman[1,2], Tahsin M. Khan[1], Justin F. Gainor[1,2], A. John Iafrate[1,4], Kengo Takeuchi[5], Makoto Taiji[6], Yasushi Okuno[7], Naoya Fujita[3], Jeffrey A. Engelman[1,2], and Alice T. Shaw[1,2]

Abstract

Purpose: The first-generation ALK tyrosine kinase inhibitor (TKI) crizotinib is a standard therapy for patients with *ALK*-rearranged non–small cell lung cancer (NSCLC). Several next-generation ALK-TKIs have entered the clinic and have shown promising activity in crizotinib-resistant patients. As patients still relapse even on these next-generation ALK-TKIs, we examined mechanisms of resistance to the next-generation ALK-TKI alectinib and potential strategies to overcome this resistance.

Experimental Design: We established a cell line model of alectinib resistance, and analyzed a resistant tumor specimen from a patient who had relapsed on alectinib. We developed Ba/F3 models harboring alectinib-resistant ALK mutations and evaluated the potency of other next-generation ALK-TKIs in these models. We tested the antitumor activity of the next-generation ALK-TKI ceritinib in the patient with acquired resistance to alectinib. To elucidate structure–activity relationships of ALK mutations, we performed computational thermodynamic simulation with MP-CAFEE.

Results: We identified a novel V1180L gatekeeper mutation from the cell line model and a second novel I1171T mutation from the patient who developed resistance to alectinib. Both ALK mutations conferred resistance to alectinib as well as to crizotinib, but were sensitive to ceritinib and other next-generation ALK-TKIs. Treatment of the patient with ceritinib led to a marked response. Thermodynamics simulation suggests that both mutations lead to distinct structural alterations that decrease the binding affinity with alectinib.

Conclusions: We have identified two novel ALK mutations arising after alectinib exposure that are sensitive to other next-generation ALK-TKIs. The ability of ceritinib to overcome alectinib-resistance mutations suggests a potential role for sequential therapy with multiple next-generation ALK-TKIs. *Clin Cancer Res; 20(22); 5686–96. ©2014 AACR.*

Introduction

The *EML4–ALK* fusion oncogene was first reported in non–small cell lung cancer (NSCLC) in 2007 (1). Approximately 3% to 5% of NSCLC tumors harbor *ALK* rearrangements. In addition to *EML4*, other fusion partners such as *TFG*, *KIF5B*, and *KLC1* have been identified in NSCLC (2–4). Fusion with any of these partner proteins is believed to mediate oligomerization of ALK, which then leads to constitutive activation of the tyrosine kinase (TK) and aberrant downstream signaling (5). As a result, ALK fusions function as potent "oncogenic drivers," and cancers harboring these rearrangements are highly sensitive to ALK kinase inhibition.

Crizotinib is a potent small-molecule inhibitor targeting cMET, ALK, and ROS1 tyrosine kinases. On the basis of its activity in phase I, II, and III clinical trials, crizotinib is approved in many countries for the treatment of advanced, *ALK*-rearranged NSCLC (6–8). Although crizotinib often induces marked and durable responses, most patients will relapse within 1 to 2 years due to the development of resistance.

Multiple different mechanisms of resistance to crizotinib have been reported previously (9–14). In approximately one third of crizotinib-resistant cases, resistance is mediated by a genetic alteration in *ALK* itself, typically a missense mutation in the tyrosine kinase domain, though amplification of the *ALK* fusion gene has also been observed. In

[1]Massachusetts General Hospital Cancer Center, Charlestown, Massachusetts. [2]Department of Medicine, Harvard Medical School, Boston, Massachusetts. [3]Cancer Chemotherapy Center, Japanese Foundation for Cancer Research, Tokyo, Japan. [4]Department of Pathology, Massachusetts General Hospital, Boston, Massachusetts. [5]Pathology Project for Molecular Targets, The Cancer Institute, Japanese Foundation for Cancer Research, Tokyo, Japan. [6]Processor Research Team, RIKEN Advanced Institute of Computational Sciences 6F, Kobe, Hyogo, Japan. [7]Graduate School of Medicine, Kyoto University, Kyoto, Japan.

Note: Supplementary data for this article are available at Clinical Cancer Research Online (http://clincancerres.aacrjournals.org/).

Corresponding Authors: Naoya Fujita, Cancer Chemotherapy Center, Japanese Foundation for Cancer Research, 3-8-31, Ariake, Koto-ku, Tokyo 135-8550, Japan. Phone: +81-3-3570-0468; Fax: +81-3-3570-0484; E-mail: naoya.fujita@jfcr.or.jp; Jeffrey A. Engelman, Massachusetts General Hospital Cancer Center, CNY 149, 13th Street, Charlestown, MA 02129. Phone: 617-724-7298; Fax: 617-724-9648; E-mail: jengelman@mgh.harvard.edu; and Alice T. Shaw, Massachusetts General Hospital Cancer Center, 32 Fruit Street, Boston, MA 02114. Phone: 617-724-4000; Fax: 617-726-0453; E-mail: ashaw1@mgh.harvard.edu

doi: 10.1158/1078-0432.CCR-14-1511

Published OnlineFirst September 16, 2014; DOI: 10.1158/1078-0432.CCR-14-1511

Translational Relevance

The ALK tyrosine kinase inhibitor (TKI) crizotinib is a standard therapy for patients with ALK-rearranged non–small cell lung cancer (NSCLC). However, cancers invariably develop resistance to crizotinib, and this has spurred the clinical development of multiple next-generation ALK-TKIs, including alectinib (RO5424802/CH5424802) and ceritinib (LDK378). To determine how cancers develop resistance to alectinib, we established a cell line model of acquired resistance to alectinib and analyzed a resistant tumor specimen from a patient who had relapsed on alectinib. We identified two novel secondary ALK mutations, both of which were still sensitive to ceritinib *in vitro*. Importantly, we found that in the patient, ceritinib was able to overcome resistance to alectinib, suggesting a potential role for sequential therapy with multiple next-generation ALK-TKIs.

contrast to *EGFR*-mutant NSCLC, in which T790M represents the sole EGFR resistance mutation in the clinic, crizotinib resistance can be mediated by a variety of different secondary mutations in ALK. To date, eight different crizotinib resistance mutations have been identified, including the gatekeeper L1196M substitution (9, 15). In some cases, resistant tumors have been found to harbor multiple nonoverlapping mutations within the ALK-TK domain (9, 11, 16). In addition, some cancers may develop resistance because the crizotinib fails to fully suppress ALK signaling despite the absence of an ALK resistance mutation (17), possibly secondary to inadequate drug exposures. Other mechanisms of crizotinib resistance appear to be independent of ALK and involve activation of alternative signaling pathways, so-called bypass tracks, such as EGFR and cKIT (11, 13, 14).

To overcome acquired resistance to crizotinib, a number of structurally distinct, next-generation ALK inhibitors have been developed and are in various phases of clinical development. In general, these drugs are more potent inhibitors of ALK and may be effective against many of the known resistance mutations, including L1196M (10, 18). Alectinib (RO5424802/CH5424802) is one of the most advanced next-generation ALK inhibitors. In preclinical studies, alectinib demonstrated strong antitumor activity against cancer cells harboring ALK fusions, both *in vitro* and *in vivo* (18). In a phase I/II study conducted in Japan, alectinib was found to be highly effective and safe in crizotinib-naïve, ALK-rearranged NSCLC, inducing responses in 94% of treated patients (19). Alectinib has also been tested in a phase I/II study in the United States. Preliminary data from this study suggest that alectinib is also highly active in crizotinib-resistant patients, with a reported response rate of 55% (24 of 44 patients; ref. 20). A similarly high response rate in crizotinib-resistant disease has also been reported with the next-generation ALK inhibitor ceritinib (LDK378; ref. 21). On the basis of these promising results, alectinib received Breakthrough Therapy Designation by the U.S. FDA, and ceritinib was recently approved by the U.S. FDA for ALK-positive patients with crizotinib-resistant or crizotinib-intolerant disease.

As with crizotinib, patients eventually develop resistance to next-generation ALK inhibitors. In this study, we have explored acquired resistance to alectinib in a cell line model and in a primary tumor specimen from an alectinib-refractory patient. We have identified two novel secondary mutations within the ALK-TK domain, both of which mediate resistance to alectinib: V1180L, which functions as a gatekeeper such as L1196M, and I1171T, which resides in the αC helix within the ALK-TK domain. The thermodynamic stability of different alectinib–ALK complexes suggests that both V1180L and I1171T substitutions cause resistance by decreasing the binding affinity of alectinib for the mutated kinases. Although cancer cells expressing either V1180L- or I1171T-mutated EML4–ALK are resistant to alectinib as well as crizotinib, they remain sensitive to other structurally distinct ALK inhibitors and to hsp90 inhibitor. Thus, two different therapeutic strategies may be effective in overcoming resistance to alectinib, including the use of an alternative next-generation ALK inhibitor in tumors with susceptible resistance mutations such as V1180L or I1171T.

Materials and Methods

Patients

The ALK-positive NSCLC patient with acquired alectinib resistance underwent biopsy of a resistant tumor in October 2012. Standard histopathology was performed to confirm the diagnosis of malignancy and the histologic subtype. Total nucleic acid was isolated as described. We also performed fluorescence *in situ* hybridization (FISH) and IHC studies as described below. The cell line was also established when we obtained sufficient tissue. The established ALK-positive patient-derived cell line has been previously tested for mutation status to confirm their authenticity. The electronic medical record was reviewed retrospectively to obtain clinical information under an Institutional Review Board (IRB)–approved protocol.

Reagents

Alectinib and LDK378 were purchased from ActiveBiochem, 17-AAG was from LC-Laboratories, NVP-TAE-684 and ASP3026 were from ChemieTek, and crizotinib was from ShangHai Biochempartner. AP26113 was from Selleck. Each compound was dissolved in DMSO for cell culture experiments.

Isolation of gDNA or total RNA preparation, sequencing of ALK fusion gene

Genomic DNA (gDNA) was isolated from cell pellets or fresh-frozen specimen with the DNeasy Blood & Tissue Kit (QIAGEN) according to the manufacturer's protocol. Total RNA was isolated from cell pellets or fresh-frozen specimen with an RNeasy Mini Kit (Qiagen) according to the manufacturer's instructions. Each exon of ALK kinase domain

Published OnlineFirst September 16, 2014; DOI: 10.1158/1078-0432.CCR-14-1511

(exon 21 to 27) or ALK kinase domain was PCR-amplified from gDNA or cDNA synthesized from total RNA with Oligo dT using KOD Plus ver.2 (TOYOBO), and sequenced bidirectionally by Sanger sequencing.

Fluorescence *in situ* hybridization

Two-color, break-apart FISH to detect *ALK* rearrangements was performed using formalin-fixed paraffin-embedded tissues with in-house ALK FISH probes [*ALK*-5′ terminal (red)/*ALK*-3′ terminal (green)] made from BAC clones. Isolated or split signals indicate *ALK* rearrangement, while overlapping signals indicate a nonrearranged *ALK* gene. Images were captured with an Olympus BX51 fluorescent microscope equipped with a charge-coupled device camera (DP71; Olympus).

Reagents and cell culture conditions

The H3122 human NSCLC cell line was obtained as previously described (22). PC9 cells were kindly provided by Dr. Kazuto Nishio (Kinki University, Osaka, Japan) and have been previously characterized (23). HCC827 was kindly provided by Dr. Adi Gazdar (University of Texas Southwestern Medical Center, Dallas, TX) and has been previously characterized (24). H460 and A549 human NSCLC cells were obtained from American Type Culture Collection. Ba/F3, immortalized murine bone marrow–derived pro-B cells were obtained from the RIKEN BRC Cell Bank (RIKEN BioResource Center). H3122, H3122-derived alectinib-resistant cells (H3122 CHR-A1), HCC827, PC9, H460, and A549 cells were cultured in RPMI-1640 supplemented with 10% FBS (R-10). Human embryonic kidney 293FT cells were cultured in DMEM supplemented with 10% FBS (D-10). Ba/F3 cells, immortalized murine bone marrow–derived pro-B cells, were cultured in D-10 with or without 0.5 ng/mL IL3 (Invitrogen).

Generation of H3122 CHR-A1 cells

H3122 CHR-A1 cells were established in the same manner as H3122 CR1 (10). Briefly, H3122 cells were seeded at approximately 50% confluence in 15-cm dishes in R-10. Alectinib was added at a starting concentration of 10 nmol/L, and cells were maintained in fresh drug-containing medium changed every 72 to 96 hours. Cells were passaged once they reached confluence. After every two passages at a given concentration of drug, the concentration of alectinib was increased until a final concentration of 1 μmol/L was achieved. The resulting pool of resistant cells (designated H3122 CHR-A1) was maintained in R-10 with 1 μmol/L alectinib.

Survival assays

For 72-hour drug treatments, 2,000 to 3,000 cells were plated in replicates of three to six into 96-well plates. Following drug treatments, cells were incubated with the CellTiter-Glo Assay reagent (Promega) for 10 minutes and luminescence was measured using a Centro LB 960 microplate luminometer (Berthold Technologies). The data were graphically displayed using GraphPad Prism version 5.0 (GraphPad Software). IC_{50} value was determined by a nonlinear regression model with a sigmoidal dose response in GraphPad.

Immunoblot analysis

Lysates were prepared as described previously (ref. 11). Equal amounts of lysates were electrophoresed and immunoblotted with the antibodies against phospho-ALK (Tyr1604), ALK (C26G7), phospho-p42/44 ERK/MAPK (Thr202/Tyr204), p42/44 ERK/MAPK, phospho-Akt (Ser473; D9E), panAkt (C67E7), phospho-S6 Ribosomal Protein (Ser240/244, D68F8), S6 Ribosomal Protein (54D2; Cell Signaling Technology), GAPDH (6C5, Millipore), and β-actin (Sigma).

Retroviral infection

cDNAs encoding EML4–ALK variant 1, EML4–ALK variant 1 V1180L, or I1171T mutants were cloned into 1,520 retroviral expression vectors (pLenti), and virus was produced as previously described (ref. 10). After retroviral infection, Ba/F3 cells were selected in puromycin (1.0 μg/mL) for 2 weeks. For Ba/F3 cells infected by EML4–ALK variants, IL3 was withdrawn from the culture medium for at least 2 weeks before experiments.

Statistical analysis

All data are shown as mean ± SD. Statistical analysis was performed using a two-tailed Student *t* test. Significance was established for $P < 0.05$.

Results

Generation and characterization of alectinib-resistant cells

The EML4–ALK–expressing NSCLC cell line H3122 is more sensitive to alectinib than crizotinib, as reported previously (Supplementary Fig. S1; ref. 11). To explore mechanisms of alectinib resistance, we generated resistant H3122 cells by exposing the sensitive parental cells to increasing concentrations of alectinib for 7 months. The fully resistant cells, H3122 CHR-A1 cells, were maintained in 1 μmol/L of alectinib. H3122 CHR-A1 cells were as resistant to alectinib as cancer cell lines that do not harbor *ALK* rearrangement (Fig. 1A and B). In contrast to parental H3122 cells, H3122 CHR-A1 cells maintained ALK phosphorylation and downstream AKT and ERK phosphorylation in the presence of 300 nmol/L of alectinib (Fig. 1C). As amplification of *ALK* fusion genes has been shown to mediate crizotinib resistance (10), we examined *ALK* gene copy number by FISH. Like the parental H3122 line, CHR-A1 cells showed no evidence of amplification of the *ALK* fusion gene (Fig. 1D).

We next examined the entire coding sequencing of EML4–ALK in both H3122 parental and CHR-A1–resistant cells. In the resistant cells, we detected a G to C substitution at nucleotide 3538 of *EML4-ALK* variant 1, which was not detected in the parental line (Fig. 1D). This 3538 G to C substitution results in a valine to leucine change at codon

Published OnlineFirst September 16, 2014; DOI: 10.1158/1078-0432.CCR-14-1511

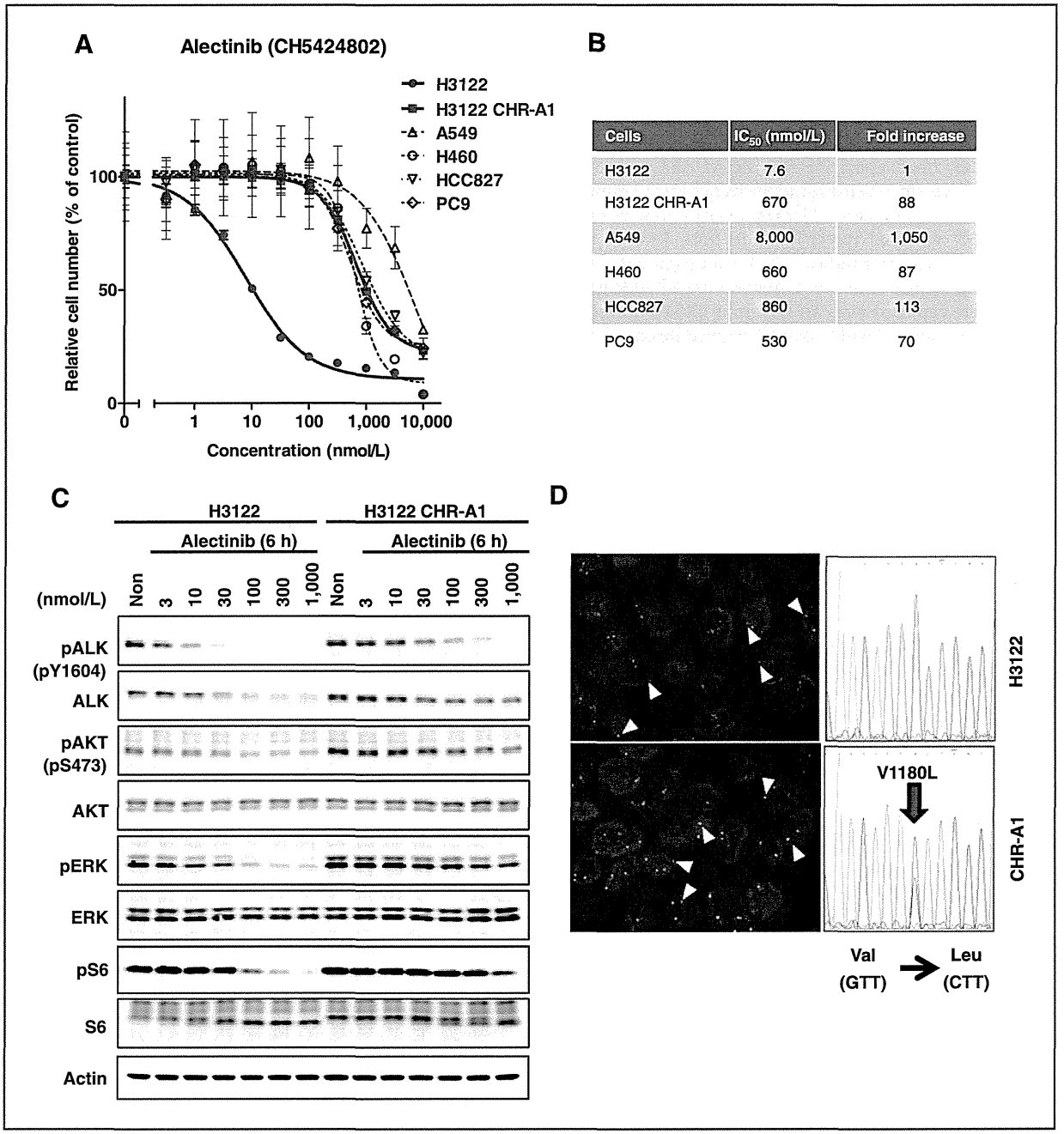

Cells	IC_{50} (nmol/L)	Fold increase
H3122	7.6	1
H3122 CHR-A1	670	88
A549	8,000	1,050
H460	660	87
HCC827	860	113
PC9	530	70

Figure 1. H3122 CHR-A1 cells are resistant to alectinib and harbor a V1180L mutation in the ALK kinase domain. A, cells were seeded in 96-well black plates and treated with increasing concentrations of alectinib for 72 hours. Cell survival was analyzed using the CellTiter-Glo Assay. Although H3122 cells showed high sensitivity to alectinib (red line), H3122 CHR-A1 cells (green line) were as insensitive to alectinib as non–ALK-rearranged cell lines. B, table summarizing IC_{50} values (nmol/L) of each cell line against alectinib. C, parental H3122 and CHR-A1 cells were treated with alectinib at the indicated concentrations for 6 hours. Cell extracts were immunoblotted to detect the indicated proteins. D, two-color FISH [ALK-5′ region (red)/ALK-3′ region (green)] analysis was performed on parental H3122 and CHR-A1 cells. Most of the cells harbor isolated or split green signals (arrowhead, EML4–ALK). Shown on the right are electrophoretograms of EML4–ALK cDNA from parental H3122 and CHR-A1 cells. The g3538c mutation within exon 23 results in a V1180L substitution that corresponds to a gatekeeper mutation in ALK.

1180 within the ALK-TK domain. On the basis of structural modeling studies of ALK (25), V1180 is predicted to lie near the L1196 gatekeeper residue, which is mutated in a subset of cell lines and patient biopsies with acquired resistance to crizotinib (9–11, 14, 16). No other tyrosine kinase mutations were detected in resistant cells.

Published OnlineFirst September 16, 2014; DOI: 10.1158/1078-0432.CCR-14-1511

Identification of a novel ALK resistance mutation in a crizotinib- and alectinib-refractory patient

To identify the mechanisms of alectinib resistance that develop in patients, we examined a resistant tumor sample from a patient with advanced ALK-positive NSCLC who had relapsed on alectinib. This patient had previously received three lines of chemotherapy and had initially responded to crizotinib, as indicated by an improvement in disease burden on CT scans. After 8 months of crizotinib therapy, the patient developed disease progression and was then treated with alectinib (300 mg twice daily). Restaging CT scans demonstrated a response to alectinib, but after 4 months, the patient again experienced disease progression, including worsening liver metastases. The patient was discontinued from alectinib, and underwent biopsy of a resistant liver lesion. Cytopathology of the tumor cells demonstrated adenocarcinoma histology, and ALK FISH analysis confirmed the presence of *ALK* rearrangement in the resistant tumor specimen. In addition, a cell line was established directly from the biopsy specimen that we designated MGH056-1.

To determine whether a secondary mutation within ALK might underlie the development of alectinib resistance in this patient, we extracted total nucleic acid from a flash-frozen specimen, and the entire tyrosine kinase domain of ALK was amplified from cDNA and sequenced. We identified a T to C missense mutation at codon 3512, leading to an I1171T amino acid substitution (Fig. 2A). The I1171 residue is located in the αC helix. Mutation of I1171 has been reported previously in neuroblastoma (26), but not in ALK-rearranged NSCLC. The MGH056-1 cell line also harbored the I1171T mutation.

To determine whether MGH056-1 cells are resistant to ALK tyrosine kinase inhibitor (TKI) therapy, we compared the sensitivity of the parental H3122, H3122 CHR-A1, and MGH056-1 cells to crizotinib and alectinib. As shown in Fig. 2B, both H3122 CHR-A1 and MGH056-1 cells were similarly resistant to crizotinib in cell viability assays. With respect to alectinib, H3122 CHR-A1 cells were highly resistant, whereas the MGH056-1 cells displayed intermediate resistance (Fig. 2B). Furthermore, compared with parental H3122 cells, MGH 056-1 cells required substantially higher concentration of alectinib (or crizotinib) to suppress the phospho-ALK and downstream signaling intermediates (compare Figs. 1C with 2C). These results suggest that I1171T-mutant ALK is relatively insensitive to both crizotinib and alectinib.

ALK I1171T and V1180L mutations mediate resistance to alectinib in Ba/F3 models

To determine whether the I1171T and V1180L mutations are sufficient to cause resistance to alectinib, we engineered Ba/F3 cells expressing EML4–ALK harboring each mutation. In cell survival assays, Ba/F3 lines expressing the mutant EML4–ALK proteins were significantly less sensitive to alectinib than those expressing wild-type (WT) EML4–ALK (Fig. 3A). Ba/F3 cells with EML4–ALK V1180L were more resistant than Ba/F3 cells with EML4–ALK I1171T (Fig. 3A), consistent with greater resistance observed in the H3122 CHR-A1 cells compared with the MGH056-1 cells. We next examined the effect of alectinib on ALK phosphorylation in the presence or absence of each resistance mutation. Consistent with the cell survival assays and the immunoblotting results with H3122 CHR-A1 and MGH056-1 cells, alectinib was much less potent at suppressing the phosphorylation of EML4–ALK harboring V1180L and, to a lesser extent, I1171T, compared with WT EML4–ALK (Fig. 3B). Thus, in Ba/F3 cells, both the V1180L and I1171T mutations confer resistance to alectinib, with V1180L appearing to confer a higher degree of resistance than I1171T.

Structural analysis of resistance mutations by computational simulation with MP-CAFEE

To understand the structure–function relationship of the two alectinib-resistance mutations in the ALK kinase domain, we performed computational simulation analysis with MP-CAFEE. To evaluate the thermodynamic stability of each complex of alectinib with WT, I1171T-, and V1180L-mutated ALK, we performed molecular dynamics simulation and estimated the free energies of each complex using MP-CAFEE method (27). Supplementary Figure S2 shows the comparison of experimental IC_{50} values and calculated free energy values. A linear correlation between experimental and calculated values was observed. This result indicates that the molecular dynamic simulation and free energy estimation by MP-CAFEE could correctly predict the resistant mechanism of each resistant mutant. In the MP-CAFEE method, the free energy value is estimated by summation of Coulomb and van der Waals potential energies. Figure 3C shows the estimated interaction energies of alectinib with WT, I1171T, or V1180L ALK. Interestingly, the decrease in binding affinities of I1171T-alectinib and V1180L-alectinib, compared with WT ALK-alectinib, are caused by decreases in Coulomb and van der Waals interactions, respectively. As shown in Fig. 3D, the I1171T mutation distorts the C-helix, shifting the position of the glutamic acid at 1167 inferiorly. As the cyano group of alectinib forms a hydrogen bond with E1167, this downward shift may disrupt binding of alectinib to the I1171T mutant. In contrast, for the V1180L mutant, our modeling predicts that the methyl group of the leucine residue clashes with the multicyclic rings of alectinib (Fig. 3D). This steric interference likely decreases the van der Waals interaction between V1180L and alectinib. Taken together, these results suggest that for both I1171T and V1180L mutations, drug resistance is due to decreased binding affinity of alectinib for the mutant kinases.

Structurally distinct next-generation ALK inhibitors overcome alectinib-resistant mutations

In addition to alectinib, several other ALK-TKIs are currently in clinical development. To determine whether these next-generation ALK inhibitors may have activity in alectinib-resistant cancers, we used the Ba/F3 cells expressing EML4–ALK harboring the I1171T or V1180L mutation. As

Published OnlineFirst September 16, 2014; DOI: 10.1158/1078-0432.CCR-14-1511

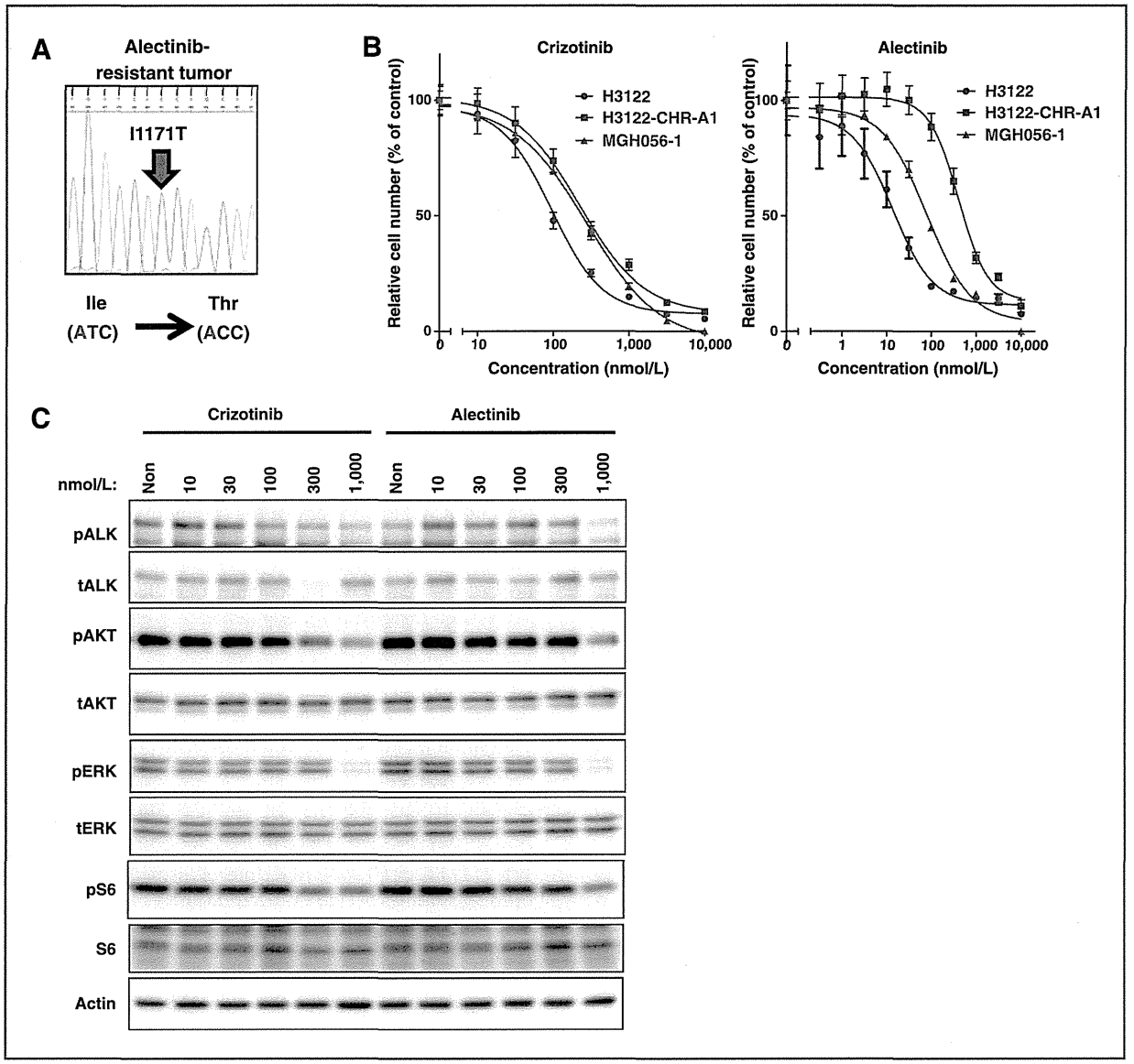

Figure 2. Discovery of the ALK I1171T secondary mutation in a patient with acquired resistance to crizotinib and alectinib. A, secondary I1171T mutation was only detected in the post-alectinib–treated specimen. Shown are electrophoretograms of ALK kinase domain cDNA from the post-alectinib treatment. B, sensitivity of MGH056-1 cells to crizotinib or alectinib. MGH056-1 cells, parental H3122, and CHR-A1 cells were treated with indicated concentrations of crizotinib or alectinib. Cell survival was analyzed with the CellTiter-Glo Assay. C, MGH056-1 cells were exposed to increasing concentrations of crizotinib or alectinib for 6 hours. Cell lysates were immunoblotted to detect the indicated proteins.

controls, we also tested Ba/F3 cells expressing WT EML4–ALK and parental, IL3-dependent Ba/F3 cells. We focused on four ALK inhibitors: the tool compound NVP-TAE684 (28), and three drugs currently in clinical trials or clinically available for ALK-rearranged NSCLC, ceritinib (LDK378; refs. 17, 21), AP26113, and ASP3026. As shown in Fig. 4A, NVP-TAE684 demonstrated potent activity against Ba/F3 cells expressing V1180L EML4–ALK or the I1171T EML4–ALK. The clinically available ALK inhibitors ceritinib and AP26113 showed slightly different selectivity profiles against the different ALK resistance mutations. Ceritinib was highly active against V1180L, even more so than against WT EML4–ALK (Fig. 4A and Supplementary Fig. S3). The I1171T mutation was also sensitive to ceritinib, demonstrating a dose-response similar to WT EML4–ALK. In contrast, AP26113 and ASP3026 were similarly active against both V1180L-mutant and WT EML4–ALK, but AP26113 was a little less active against I1171T-mutated EML4–ALK, whereas ASP3026 was inactive against I1171T (Supplementary Figs. S3 and S4). The suppression of phospho-ALK by the different inhibitors across the various mutations was consistent with the potencies observed in these Ba/F3

Published OnlineFirst September 16, 2014; DOI: 10.1158/1078-0432.CCR-14-1511

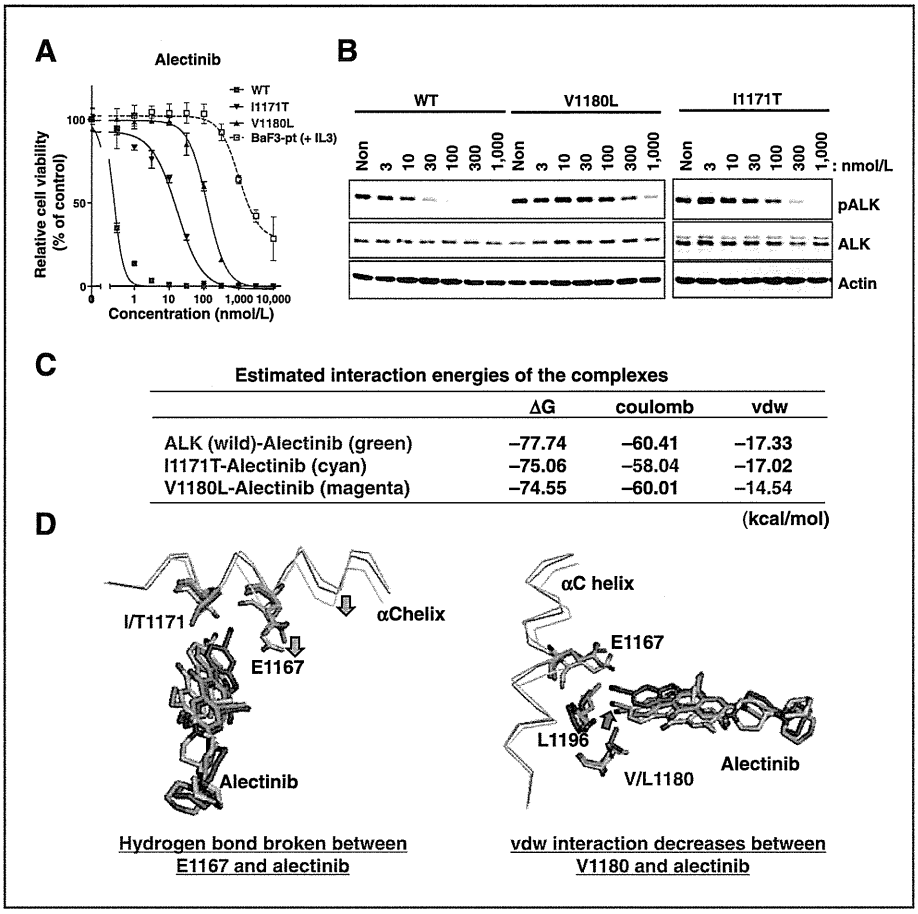

Figure 3. Biochemical and structural basis of alectinib resistance mediated by ALK I1171T and V1180L mutations. A, Ba/F3 cells expressing WT, I1171T, or V1180L EML4–ALK were seeded in 96-well plates and treated with the indicated concentrations of alectinib for 72 hours. Cell viability was analyzed using the CellTiter-Glo Assay. B, inhibition of phospho-ALK by alectinib in Ba/F3 models. WT or mutated EML4–ALK–expressing Ba/F3 cells were exposed to increasing concentrations of alectinib for 2 hours. Cell lysates were immunoblotted to detect the indicated proteins. C, estimated interaction energies of the indicated complexes [alectinib with WT ALK (green), ALK I1171T (cyan), or ALK V1180L (magenta)] by MP-CAFEE methods are shown. In the MP-CAFEE methods, the free energy value (ΔG) is estimated by summation of coulomb and van der Waals (vdw) potential energies. D, shown are the complex average structures in the equilibrated molecular dynamics simulation for WT ALK (green), ALK I1171T (cyan), and ALK V1180L (magenta).

studies (Supplementary Figs. S3 and S5). These results suggest that at least two of the next-generation ALK inhibitors—ceritinib and AP26113—may be able to overcome resistance to alectinib mediated by either I1171T or V1180L mutations.

We next tested the efficacy of several ALK inhibitors (TAE-684, crizotinib, and ceritinib) in alectinib-resistant H3122 CHR-A1 cells harboring the V1180L EML4–ALK mutation. Parental H3122 cells, as well as *KRAS*- or *EGFR*-mutant cancer cell lines (A549, H460, PC-9, and HCC827), were used as controls. As shown in Fig. 4B, TAE-684 markedly suppressed cell growth in both sensitive H3122 and alectinib-resistant H3122 CHR-A1 cells, but had almost no effect on the viability of other, non–ALK-dependent cancer cell lines. TAE-684 suppressed ALK phosphorylation and downstream signaling (Fig. 4C, left), and induced apoptosis (Supplementary Fig. S6). In contrast, crizotinib treatment was significantly less effective against H3122CHR-A1 cells compared with H3122 parental cells (Fig. 4B and C). Like TAE-684, ceritinib demonstrated potent activity against both parental H3122 and alectinib-resistant H3122 CHR-A1 cells, decreasing cell growth (Fig. 4B), suppressing ALK phosphorylation (Fig. 4C), and inducing apoptosis (Supplementary Fig. S6).

The hsp90 inhibitor 17-AAG overcomes alectinib resistance in H3122 CHR-A1 cells

A number of hsp90 inhibitors have demonstrated clinical activity in ALK-rearranged NSCLC, including in 1 patient with acquired resistance to crizotinib (29, 30). We therefore tested whether the alectinib-resistant H3122 CHR-A1 cells might be sensitive to the hsp90 inhibitor 17-AAG. Compared with *KRAS* or *EGFR*-mutant cancer cell lines (A549, H460, PC-9, and HCC827), CHR-A1 cells were highly sensitive to 17-AAG treatment, and nearly as sensitive as parental H3122 cells (Supplementary Fig. S7). On the basis of immunoblotting, 17-AAG treatment reduced EML4–ALK protein levels in both parental H3122 and H3122CHR-A1 cells to similar extents, as well as downstream signaling. Thus, Hsp90 inhibition may represent an alternative therapeutic strategy for overcoming resistance to alectinib due to acquisition of a resistance mutation.

Ceritinib is active in a cell line model and a patient with alectinib resistance

We also tested the efficacy of different ALK inhibitors in the MGH056-1 cells. As shown in Fig. 5A, ceritinib, but not crizotinib or alectinib, markedly suppressed the cell growth of MGH056-1 cells. Ceritinib also suppressed ALK

Published OnlineFirst September 16, 2014; DOI: 10.1158/1078-0432.CCR-14-1511

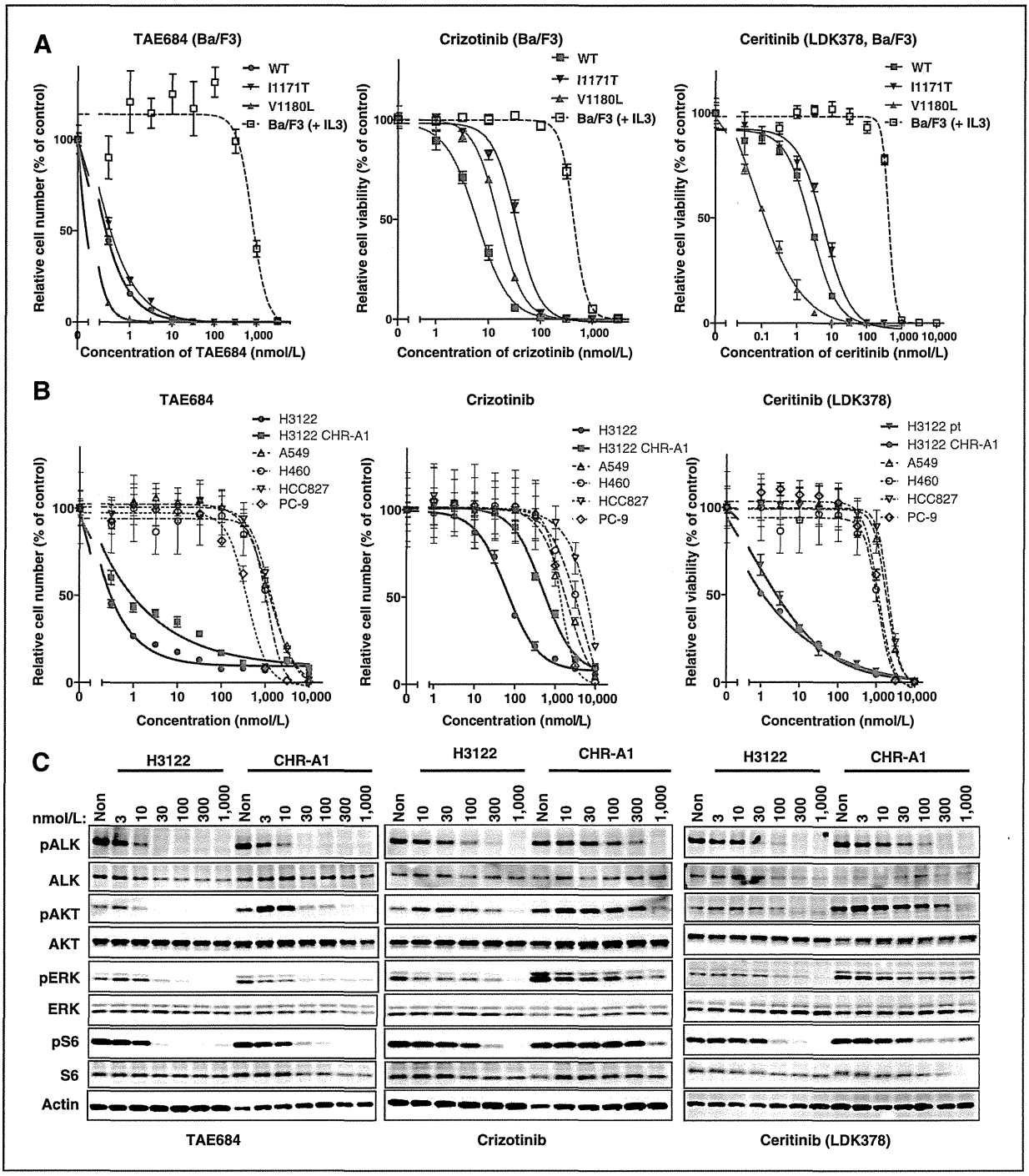

Figure 4. Ceritinib overcomes alectinib resistance in Ba/F3 models and H3122 CHR-A1 cells. A, parental Ba/F3 cells and Ba/F3 cells expressing WT, I1171T, or V1180L EML4–ALK were seeded in 96-well plates and treated with the indicated concentrations of TAE-684 (left), crizotinib (center), or ceritinib (right) for 72 hours. Cell viability was analyzed using the CellTiter-Glo Assay. B, cancer cell lines, including parental H3122 and alectinib-resistant H3122 CHR-A1 cells, were seeded in 96-well plates and treated with increasing concentrations of TAE-684 (left), crizotinib (center), or ceritinib (right) for 72 hours. Cell viability was measured using the CellTiter-Glo Assay. Both parental H3122 cells and H3122 CHR-A1 cells showed marked sensitivity to TAE-684 and ceritinib. Non–ALK-rearranged cell lines (A549, H460, HCC827, and PC-9 cells) showed minimal growth inhibition when exposed to ALK inhibitors. C, suppression of ALK signaling by ALK inhibitors (TAE684, crizotinib, or ceritinib) in parental H3122 and CHR-A1 cells. Cells were exposed to increasing concentrations of TAE684, crizotinib, or ceritinib for 6 hours. Cell lysates were immunoblotted to detect the indicated proteins.